LOW-TEMPERATURE SOLUTION SYNTHESIS OF ALLOYS AND INTERMETALLIC COMPOUNDS AS NANOCRYSTALS

A Dissertation

by

YOLANDA VASQUEZ

Submitted to the Office of Graduate Studies of
Texas A&M University
in partial fulfillment of the requirements for the degree of

DOCTOR OF PHILOSOPHY

December 2008

Major Subject: Chemistry

LOW-TEMPERATURE SOLUTION SYNTHESIS OF ALLOYS AND INTERMETALLIC COMPOUNDS AS NANOCRYSTALS

A Dissertation

by

YOLANDA VASQUEZ

Submitted to the Office of Graduate Studies of
Texas A&M University
in partial fulfillment of the requirements for the degree of

DOCTOR OF PHILOSOPHY

Approved by:

Chair of Committee,	Raymond E. Schaak
Committee Members,	Marcetta Y. Darensbourg
	Kim R. Dunbar
	Joseph Ross
Head of Department,	David H. Russell

December 2008

Major Subject: Chemistry

ABSTRACT

Low-Temperature Solution Synthesis of Alloys and Intermetallic Compounds as Nanocrystals. (December 2008)

Yolanda Vasquez, B.S., The University of Texas at El Paso

Chair of Advisory Committee: Dr. Raymond E. Schaak

The synthesis of solid state materials has traditionally been accomplished using rigorous heating treatments at high temperatures (1,000°C) to overcome the slow rate of diffusion between two reactants. Re-grinding and re-heating treatments improve the rate of reaction between two solids; however, the high temperatures required to overcome the diffusion barrier limit the products accessible to the most thermodynamically stable phases. In this work, nano-scale solids such as alloys and intermetallics were synthesized via solution techniques where metal compounds are reduced by $NaBH_4$ or n-butyllithium at temperatures below 300°C.

To form hollow particles, metal nanoparticles of Co, Ni, Pb were synthesized via reduction by $NaBH_4$ in water and reacted with K_2PtCl_6, which resulted in the formation of alloys in the case of Co-Pt and Ni-Pt. PbPt intermetallic hollow particles were synthesized by heating a composite of PbO and hollow Pt nanoparticles in tetraethylene glycol (TEG) at 140 °C. With n-butyllithium as a reducing agent, Au_3M (M= Fe, Co, Ni) nanoparticles could be synthesized as isolatable solids in the $L1_2$ structure. PtSn and $AuCu_3$ intermetallics were synthesized using $NaBH_4$ and TEG. The PtSn and $AuCu_3$

nanoparticles were characterized by transmission electron microscopy in attempts to learn about the phase diagrams of nanoscale solids.

The purpose of this work was to synthesize nanoparticles via solution-mediated routes at low temperatures in compositions and morphologies not observed in the bulk, and learn about the phase diagrams of nanoparticles to understand why it is possible to access solids at temperatures significantly below those used in traditional solid state chemistry.

DEDICATION

I dedicate this dissertation to my husband and daughters for bringing so much joy into my life; to my mother, my sisters, and all my family for their support.

ACKNOWLEDGEMENTS

I would like to thank my graduate advisor, Prof. Raymond E. Schaak, for all his help and guidance throughout my graduate career. I would like to thank Prof. Marcetta Y. Darensbourg for mentoring me and my committee members, Prof. Kim R. Dunbar and Prof. Joseph Ross for their positive feedback and support. I also thank Dr. Zhiping Luo and Prof. Andreas Holzenburg for their guidance throughout the course of this research.

Thanks also to my friends and colleagues and the department faculty and staff for making my time at Texas A&M University both a humbling and a great experience. Finally, thanks to my husband and daughters for their patience and love and to my mother and sisters for their encouragement.

TABLE OF CONTENTS

CHAPTER Page

LIST OF FIGURES

Page

CHAPTER I

INTRODUCTION: SOLUTION BASED STRATEGIES FOR THE SYNTHESIS OF ALLOYS AND INTERMETALLICS*

When solids are dimensionally confined in the nanometer size regime, many interesting characteristics emerge that can be different from bulk analogues of the same material. One classic example is quantum dots, in which the carriers or excitons are confined in three dimensions and whose optical properties vary as a function of size.[1] Similarly, the optical properties of gold nanoparticles can be tuned by adjusting the nanoparticle shape and size due to surface plasmon resonance effects.[2-4] The properties of many other materials change upon dimensional confinement as well, including magnetism,[5,6] catalysis,[7,8] and mechanical properties.[9,10] Importantly, the unique properties of nanoscale solids can be harnessed for a variety of applications, including information storage,[11,12] medical and biological imaging,[13-15] and catalysis for energy[16-18] and chemical[19,20] applications. Because of their size and solubility, nanoscale solids are also ideal precursors to thin films,[21-23] functional devices,[24] coatings,[25-27] and templated materials[28-30] that can be formed using inexpensive benchtop solution process procedures.

This dissertation follows the style of the *Journal of the American Chemical Society*.

A large number of methods have been developed for synthesizing nanocrystalline solids. Physical "top down" methods such as ball milling[31,32] and laser ablation[33] are among the most straightforward, since they involve the direct size-reduction of already-made solids. While general for many classes of solids, it can be extremely difficult to control size, size dispersity, and morphology using these methods, which limits their utility. Other common synthetic strategies for nanocrystalline solids include gas-phase condensation,[34,35] sputtering,[36,37] and flame hydrolysis.[38,39] Thin film deposition and annealing methods can also be used to form nanoparticles supported on a substrate.[40]

Chemical methods are also widely used for synthesizing nanocrystalline solids.[41,42] Among the variety of techniques used, the most common involve reduction of metal salt precursors,[41] thermal decomposition of metal-organic complexes,[43,44] co-precipitation,[45] nucleation within inverse micelles or microemulsions,[46,47] and solvothermal reactions.[48] Typically reactions are performed in the presence of organic stabilizers, which help to passivate the nanocrystal surface[49,50], control its size and surface chemistry for solubility and surface accessibility,[51,52] and influence growth directions to facilitate shape control.[53,54] Under appropriate conditions, solution methods allow for tight control over the size and size dispersity of nanoparticles, as well as their shape.[55-57] Gram-scale quantities of nanocrystals can also be produced.[58,59]

Because of these synthetic challenges, most high quality nanocrystals prepared using solution chemistry methods are limited to relatively simple solids. Most high quality nanocrystals that have been reported fall into a handful of categories with a few well-studied targets in each, such as transition metals (e.g. Au, Ag, Pt, Pd, Co), metal

oxides (e.g. ZnO, Fe_3O_4, TiO_2), and metal chalcogenides (e.g. CdS, CdSe, ZnS). For example, it is possible to use direct solution chemistry methods to generate metal nanocrystals with shapes that include spheres,[60,61] cubes, [62,63] triangles,[64,65] hexagonal platelets,[64] disks,[66] tetrahedra,[67,68] octahedra,[69,70] multipods,[71,72] rods,[73,74] wires,[73] and right-bipyramids.[67] These and other systems that are reaching synthetic maturity have been chosen and studied for good reason, e.g. important size-dependent physical properties that are interesting targets for scientific study and also useful for emerging applications. However, from the perspective of solid state chemistry, these systems are primitive – primarily single elements, simple alloys, metal oxides with one or two metals, and single metal chalcogenides.

Applying the same synthetic concepts to more complex solids is challenging, since homogeneous co-nucleation of two, three, or more elements with controlled composition and phase formation (crystal structure) is required in a nanometer-scale solid using soluble metal salts or metal complexes that typically have different reduction potentials, reduction kinetics, decomposition temperatures, ligand binding affinities, reactivities, electronegativities, etc. Superimposed on this challenge is shape control, which further requires different growing crystal faces to be selectively stabilized and destabilized to facilitate anisotropic (non-spherical) growth.

Developing synthetic strategies to access more complex alloys and intermetallic compounds can be achieved using low temperature techniques. Intermetallic compounds represent a subset of alloys that tend to have fixed stoichiometric compositions and atomically ordered crystal structures, in contrast to alloys that are crystalline solid

solutions, which usually exist over a range of compositions. Many types of chemical reactions are applicable to nanocrystal systems, providing a toolbox of techniques to form nanocrystals with morphological, compositional, or structural features that are otherwise challenging or impossible to prepare. Among these reactions are galvanic replacement, transmetallation, oxidation, and diffusion reactions. The main types of reactions that are observed in the synthesis of nanoscale alloys and intermetallics are galvanic replacement reactions and diffusion reactions, which depending on the reaction conditions, can be largely classified as "conversion chemistry". The concept of conversion chemistry is to use nanocrystals that are straightforward to synthesize as templates and convert them, via chemical reactions, into different types of nanocrystals (i.e. alloys and intermetallics). The nanocrystal ''reactants'' serve as compositional, and in many cases morphological, templates that help to define the composition and morphology of the ''product'' nanocrystals.

Galvanic replacement reactions are widely used to template the formation of metal or alloy nanocrystals[55,75] (Figure 1). These reactions proceed by sacrificially oxidizing a core metal nanocrystal by reacting it with a metal salt species that has a more positive reduction potential. Hollow nanocrystals, which have nanocrystalline shells with no material in the center, are desirable for catalysis because of their increased surface area and their minimal use of metals in the actual nanocrystal, which is particularly important for expensive catalytic elements such as Pt and Au.

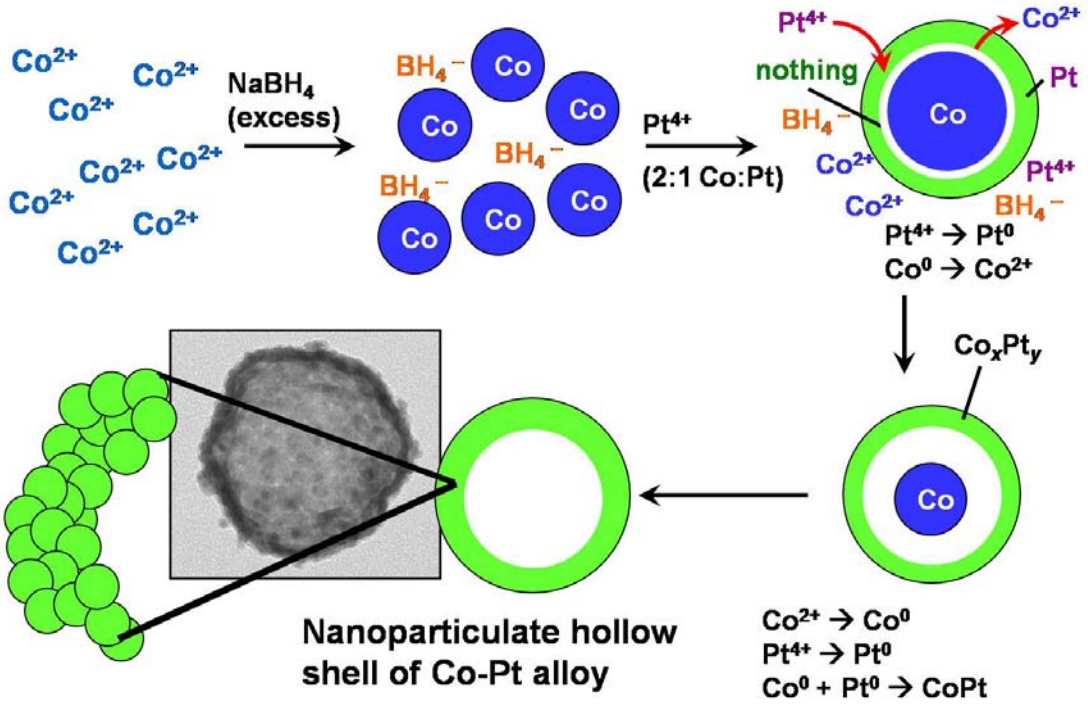

Figure 1. Scheme of hollow particles formed through galvanic replacement reactions. Co nanoparticles are produced via $NaBH_4$ reduction. Pt cations are reduced on the surface of Co nanoparticles to form a shell. Continual reduction and oxidation between the Co core and Pt shell results in the formation of an alloyed hollow shell.

Nanocrystals of intermetallic compounds can be synthesized using solution chemistry methods via diffusion reactions. The polyol process coupled with "conversion chemistry" has been a successfully solution route to synthesize various alloys and intermetallics. The concept of conversion chemistry became apparent while studying the formation of nanoparticles of the ternary intermetallic compounds $AuMSn_2$ (M = Cu, Ni) via a modified polyol process. Originally synthesized in a one-pot reaction,[76] careful investigation of the reaction pathway revealed that Au nanoparticles formed first, followed by diffusion of Sn into the Au to form nanoparticles of the intermetallic compound AuSn.[77,78] Continued heating in the presence of additional Sn and Cu

converted the AuSn nanoparticles into $AuCuSn_2$. DiSalvo and co-workers observed a similar metal intermediate in the formation of PtBi nanoparticles, where Bi was formed first and allowed to react with Pt that was added separately.[78] This insight has opened the door to a large number of intermetallic compounds that are accessible as nanoparticles using solution chemistry routes. Importantly, using preformed metal nanoparticles as reactive templates has provided a pathway to shape-controlled intermetallic nanocrystals, which are quite rare[79] and have remained a formidable synthetic challenge despite similar achievements for shape-controlled nanocrystal synthesis of other classes of solids. For example, shape-controlled nanocrystals of β-Sn can be converted to M-Sn intermetallic nanocrystals under conditions that maintain the shape defined by the β-Sn template.[80] The result is nanocrystals of $FeSn_2$ with shapes that include spheres, cubes, hollow squares, U-shaped structures, nanorods, and nanorod dimers. These nanocrystals are formed by reacting similarly shaped β-Sn nanocrystals with a solution of $FeCl_3$ under reducing conditions. This reaction facilitates reduction and diffusion of the Fe into the β-Sn. The structural relationship between β-Sn and $FeSn_2$ likely contributes to the retention of shape and crystallinity. The anisotropic structure of β-Sn, and the resultant different diffusion rates along the a and b axes, facilitates an anisotropic Kirkendall effect that yields interesting hollow nanocrystals, including hollow squares and U-shaped structures, as well as nanorods via Kirkendall mediated cleavage of cube-shaped β-Sn nanocrystals.[80] Single-crystal nanorods in a large number of intermetallic systems ($CoSn_3$, Ni_3Sn_4, Cu_6Sn_5, Ag_4Sn, AuSn, PtSn, $RuSn_2$) can also be synthesized via diffusion-based conversion of β-Sn nanorods using similar chemistry.[81] Interestingly,

and separate from the goal of generating shape controlled intermetallic nanocrystals via low temperature solution synthesis and conversion chemistry, is the discovery that a variety of compounds that are traditionally difficult to prepare in bulk form can be readily accessed using this chemical strategy. For example, while the Co–Sn binary phase diagram was established decades ago, α-$CoSn_3$ was only discovered about 10 years ago.[82,83] α-$CoSn_3$ is a low-temperature intermetallic compound that is only stable up to 275 °C, and can be formed in bulk using either a peritectic reaction or a tin flux.[82,83] While α-$CoSn_3$ can clearly form as a bulk solid, including in single-crystal form, it is not the easiest phase to access in the Co–Sn system. In contrast, when using the nanocrystal solution conversion chemistry approach, α-$CoSn_3$ is reproducibly the easiest phase to form in the Co–Sn system.[80] It is well known that nanoparticles can stabilize phases that are not thermodynamically stable or that are stable only at low temperatures. Similarly $RuSn_2$, which is reported in the literature to be a metastable phase that is difficult to synthesize, also appears to form reproducibly as hollow nanorods upon reaction of β-Sn nanorods with $RuCl_3$ in tetraethylene glycol at 200 °C under reducing conditions.[81]

In the following chapters, strategies to synthesize hollow CoPt, NiPt, and PbPt nanoscale alloyed and intermetallic materials and non-equilibrium Au based intermetallics in solution will be presented as well as a study of how the composition of AuCu and PtSn intermetallic nanoparticles is affected by these low temperature solution based strategies. Chapter II focuses on the use of sacrificial metal nanoparticles to synthesize alloyed and intermetallic nanoparticles via galvanic replacement reactions. Ni

and Co metal nanoparticles serve as the templates and form hollow particles when reacted with a Pt salt. Hollow intermetallic PbPt nanoparticles could be synthesized by a two step process in which Pb nanoparticles are reacted in water with a Pt salt to form hollow nanoparticles, and subsequently, isolated and heated in a high boiling solvent such as tetraethylene glycol (TEG) to 120°C. Overall shape and size retention of the template material is observed in the final nanoparticle products that are converted to hollow particles in water. Hollow networks are observed in the case of PbPt intermetallic nanoparticles.

Chapter III highlights the synthesis of intermetallic compounds of Au with the 3*d* transition metals Fe, Co, and Ni, which are non-equilibrium phases that have many useful potential applications as catalytic, magnetic, optic, and multifunctional magneto-optic materials. However, the atomically ordered Au−M (M = Fe, Co, Ni) intermetallics are particularly elusive from a synthetic standpoint. The Au_3Fe, Au_3Co, and Au_3Ni $L1_2$ (Cu_3Au-type) intermetallic compounds are synthesized using *n*-butyllithium as a reducing agent at temperatures as low as 240°C. Reaction pathway studies for the Au_3Co system indicate that Au nucleates first, followed by Co incorporation to form the intermetallic. The non-equilibrium intermetallic nanocrystals are characterized by powder XRD, TEM, EDS, selected area electron diffraction, and nanobeam electron diffraction, which collectively confirm the compositions and superlattice structures.

Chapter IV covers transmission electron microscopy (TEM) studies of $AuCu_3$ and PtSn nanoparticles. These systems have been synthesized through the modified polyol process. Low temperature synthesis of these particles could, however, allow for a

higher tolerance in the variance in composition as nanoscale intermetallics. $AuCu_3$ nanoparticles are known to nucleate via a conversion pathway and PtSn nanoparticles were synthesized through a two step conversion technique where Pt nanoparticles were reacted with $SnCl_2$ in TEG. The goal in this study is to determine whether, as nanocrystals, $AuCu_3$ and PtSn are truly adhering to the behavior of the traditional bulk-phase diagrams. The $AuCu_3$ system is an umbrella phase in bulk where significant variation in the stoichiometry is tolerated and results in the $L1_2$ structure. PtSn is a line phase in bulk and large differences in the stoichiometry would result in a phase separated structure.

CHAPTER II

SYNTHESIS OF ALLOYED AND INTERMETALLIC HOLLOW PARTICLES*

INTRODUCTION

Hollow nanospheres have emerged as intriguing materials for diverse applications that include drug delivery,[84,85] bioencapsulation,[86,87] medical diagnostics,[88] catalysis,[89] plasmonics,[90] and composite electronic and structural materials.[91] Hollow metal nanostructures are particularly interesting, as they can often impart multiple functionalities on a single particle. For example, hollow Au nanospheres have tunable plasmon resonances and well-established surface chemistry, making them appropriate for use in photothermal drug delivery[92] and as contrast agents.[88] Hollow metal nanospheres are often synthesized using sacrificial templates, such as polymer or SiO_2 spheres, which define the shape and size of nanoshells that are generally deposited using layer-by-layer[93] or electroless deposition methods.[94] Galvanic displacement reactions that exploit differences in the reduction potentials of two or more metals can also be used to prepare hollow metal nanostructures.[55,95-98] Despite recent advances in

*Reprinted in part with permission from "One-pot Synthesis of Hollow Superparamagnetic CoPt Nanospheres" by Vasquez, Y.; Sra, A. K.; Schaak, R. E., 2008, *J. Am. Chem. Soc.*, 127, 1509-1510. Copyright [2005] by the American Chemical Society. Also reprinted with permission from "Nanocrystal Conversion Chemistry: A Unified and Materials-General Strategy for the Template-Based Synthesis of Nanocrystalline Solids," by Vasquez, Y.; Henkes, A.E.; Bauer, J. C.; Schaak, R. E., 2008, *J. Solid State Chem.* 181, 1509-1524. Copyright [2008] by Elsevier**.**

synthesizing metal nanostructures with controlled morphologies, there are very few reports of bimetallic hollow nanospheres.[97,98,99] Bimetallic systems often offer advantages over single-metal systems. For example, metal alloy nanoparticles can show enhanced catalytic activity and selectivity relative to their single-metal components,[100,101] and both optical[102] and magnetic[44] properties can be fine-tuned by adjusting the metal ratios in alloy nanoparticles.

Ag nanoparticles have been used to form hollow Au and Pt nanoparticles in aqueous and organic media. Xia and co-workers used monodisperse poly(vinyl)pyrollidone (PVP) stabilized Ag nanocubes to produce hollow Au nanocubes or nanoboxes (~100 nm) when reacted with aqueous $HAuCl_4$.[55,56] Other morphologies of Au could also be accessed including triangles, rods, wires, and spheres, as well as Pt and Pd hollow wires.[95] In contrast to the aqueous reaction, Yin et al. found that when smaller Ag nanoparticles (~ 10 nm) were used as templates in organic media, the exterior shape of the Au hollow structure changed from spherical to faceted or truncated octahedral.[103] Interestingly, multi-faceted Ag nanoparticles reacted with $HAuCl_4$ in chloroform resulted in AgAu alloys with nanoring or nanocage morphologies.[104] Sastry et al. synthesized Au and Pt hollow spheres by a phase transfer reaction of Ag nanoparticles into chloroform using octadecylamine (ODA) followed by phase transfer of aqueous $HAuCl_4$.[105] Pt hollow spheres were formed in the same manner except benzyldimethylstearylammonium chloride was used as the phase transfer agent.[105] Co nanoparticles synthesized by $NaBH_4$ reduction have also been used as templates to synthesize hollow Au spheres,[106] Pt spheres,[107] and Au/Pt bimetallic tubular

nanoparticles.[99] Under an applied magnetic field Co nanoparticles were aligned in a chain and used as a template to form hollow chains of Pt, Au, and Pd.[108]

Metal nanoparticles can be converted to alloys, typically through galvanic replacement reactions or through conversion of isolatable metal intermediates in one-pot reactions. Galvanic replacement reactions that use pre-made metal nanocrystals as precursors are particularly powerful, because they often provide a mechanism for controlling the morphology of the alloy nanocrystal products. For example, AgAu alloys can be synthesized by reacting pre-formed Ag nanoparticles with aqueous $HAuCl_4$ to produce nanoboxes,[109] nanocages,[110] and multi-walled nanotubes[111] with tunable surface plamon resonance (SPR) bands. This technique has been extended to even more complex nanostructures, including multi-walled AgAu/AgPd nanotubes[75] and hollow nanoboxes of AgPd and AgPt alloys.[109] Although the formation of the AgAu alloys was initially observed as an intermediate step in the synthesis of hollow Au nanoparticles[112], the degree of alloying can be controlled in the hollow structures[112] as well as in dense analogs.[113] Subsequent work led to the synthesis of hollow AgAu nanoparticles in chloroform.[104] Hollow nanocages with pinholes and ring-like structures were observed when multiply twinned oleylamine stabilized Ag nanoparticles were reacted with $HAuCl_4$ in chloroform. Galvanic replacement reactions have been used to synthesize other alloy nanocrystals. For example, Liang et al.[114] synthesized Au–Pt bimetallic nanoparticles with hollow linearly aggregated morphologies using magnetic Co nanoparticles as sacrificial templates.

In this chapter we report the synthesis of hollow magnetic CoPt nanospheres synthesized through a novel and potentially general one-pot reaction that exploits an in situ sacrificial template. We describe the use of metal nanoparticles as morphological templates to form alloys of CoPt and NiPt as well as hollow nanoparticles of intermetallic PbPt. Alloys of Co-Pt and Ni-Pt are important targets since hollow nanospheres of these systems could find widespread use in magnetic, catalytic, and biomedical applications. Intermetallic PbPt nanoparticles have been shown to be electrocatalytically active towards formic oxidation[115] and, for this reason, this system was also chosen as a target to study. Unlike alloys, in which the atoms are disordered in the crystal structure, intermetallic compounds have an ordered structure with unique atomic positions and exhibit properties which are often different or enhanced relative to the alloys. Intermetallic hollow nanosheres could have many potential applications as catalysts due to cost reduction, enhanced catalytic activity due to ordering, and high surface area.

EXPERIMENTAL SECTION

Chemicals. All chemicals purchased from Alfa Aesar and were used as received. The chemicals used were: $CoCl_2 \cdot 6H_2O$, poly(vinyl pyrrolidone) (PVP, MW = 40, 000, 8, 000, and 630, 000), tetraethylene glycol (TEG) , $NaBH_4$, K_2PtCl_6, $NiCl_6 \cdot xH_2O$, $Pb(Ac)_2$ (Ac = acetate), $Pt(acac)_2$ (acac = 2, 4- pentanedionate), and PEO (poly(2-ethyl-2-oxazoline)).

Synthesis of hollow spheres in water. In a typical synthesis of CoPt hollow spheres, $CoCl_2 \cdot 6H_2O$ (8.5 mg) and poly(vinyl pyrrolidone) (PVP, MW 40 000, 100 mg) are

dissolved in 50 mL of NANOpure H_2O (18.2 MΩ), sonicated for 15 min, and purged with Ar for 15 min. A freshly prepared solution of $NaBH_4$ (10 mg in 20 mL of H_2O) is then added dropwise with stirring. Immediately after all of the $NaBH_4$ has been added, K_2PtCl_6 (16.4 mg in 20 mL H_2O) is added drop-wise with stirring. After 30 min, the product is collected by centrifugation, washed several times with H_2O and ethanol, and dried under ambient conditions. NiPt hollow spheres were synthesized using a similar procedure except $NiCl_6 \cdot xH_2O$ was used instead of $CoCl_2 \cdot 6H_2O$.

Synthesis of PbPt intermetallic nanospheres. In an Erlenmeyer flask, 100 mg of poly(vinyl) pyrrolidone (PVP, 40, 000 MW) and 11 mg (.034 mmol) of $Pb(Ac)_2$ were dissolved in 50 mL of Nanopure™ filtered water. After degassing with Ar, 20 mL of a 1.1 mM solution of $NaBH_4$ was rapidly added drop-wise followed by drop-wise addition of 20 mL of a 1.34 mM solution of K_2PtCl_6. After 20 min., the reaction was centrifuged at 3, 900 RPM, followed by washing with Nanopure water and ethanol. The pellet of Pt hollow particles was dried in Ar and redispersed in 0.5 mL of TEG. This solution of hollow particles was dispersed in 0.5 mL of TEG was added to hot TEG (120˚C) and allowed to heat for 5-15 min. After heating for 5-15 min, the hot TEG solution was then quenched in RT ethanol and centrifuged at 13, 900 RPM. The Pt hollow spheres from the intitial reaction in water could be added at various temperatures, amounts of TEG, and PVP to find the best conditions to obtain hollow intermetallic PbPt nanoparticles. Procedures for the synthesis of PbPt nanoparticles made solely by the modified polyol process were also attempted. In these experiments the goal was to synthesize the Pb nanoparticles (via reduction with $NaBH_4$) and react them with K_2PtCl_6 in TEG at

temperatures above 120 °C where the NiAs type PbPt is formed. In a typical reaction, 100 mg of PVP (MW = 40, 000) were dissolved in 20 mL of TEG and heated above 200 °C, a temperature that has been shown to form discrete Pb colloids. $Pb(Ac)_2$ was dissolved in 5 mL of TEG and added via syringe at this temperature, followed by a solution of 10 mg of $NaBH_4$ in 5 mL of TEG, and 16.4 mg of K_2PtCl_6 in 10 mL of TEG. The reaction was allowed to heat for 5-1h time intervals.

Characterization. Powder X-ray diffraction (XRD) data were collected using a Bruker GADDS three-circle X-ray diffractometer using Cu Kα radiation and microdiffraction powder techniques. Transmission electron microscopy (TEM) images, selected area electron diffraction (SAED) patterns, and energy-dispersive X-ray spectroscopy (EDS) were collected on a JEOL JEM-2010 TEM. Samples were prepared by re-suspending the isolated and cleaned nanospheres in ethanol and dropping the solution on a carbon coated Cu grid. Element mapping images were obtained using a semi-STEM (STEM = scanning transmission electron microscopy) attachment. Magnetic susceptibility measurements were obtained using a Quantum Design SQUID MPMS-XL magnetometer by cooling the sample from 300 – 5 K in a 10, 000 Oe field. Hysteresis loops (magnetization vs. applied field) were collected from 0 – 6.5 T at 5 K. X-ray photoelectron spectroscopy (XPS) measurements were obtained using a Kratos Ultra Axis His 165 XPS with an Al anode set at 15 mA and 15 kV. Samples for XPS analysis were prepared by sonicating the nanospheres in ethanol, dropping a dilute suspension on a clean Si wafer, and then drying. High-quality scans were obtained for the Pt 4f regions ($4f_{5/2}$ and $4f_{7/2}$ peaks) and compared to control experiments on bulk Pt and PVP-

stabilized Pt nanoparticles. (The Pt 4f peaks for the hollow CoPt nanospheres were shifted relative to both bulk Pt and the Pt nanoparticles prepared by the same method, showing further evidence for alloy formation.)

RESULTS AND DISCUSSION

Hollow spheres synthesized in Nanopure water

Figure 2 shows Transmission electron microscope (TEM) images of CoPt hollow spheres produced by varying the mole ratios of Co:Pt. The $Co_{50}Pt_{50}$ alloy was obtained when a 2:1 Co:Pt mole ratio was used. Figure 2a shows hollow particles formed using a 1:1 mol ratio of Co: Pt which produced hollow particles with a stoichiometry of less than $Co_{50}Pt_{50}$. When the mole ratio of Co:Pt was increased to 3:1 and 4:1, the amount of Co incorporated into the CoPt hollow shells did not increase and instead fewer hollow particles with a hollow morphology were observed. TEM images of $Co_{50}Pt_{50}$ hollow spheres are shown in Figure 2b. The reaction appears to form hollow spheres with average diameters of 10-50 nm in yields of 70-90% (see Figure 3). Particles smaller than 20 nm look cracked and chains of CoPt nanoparticles are observed due to magnetic dipole interactions. The individual nanosphere shown in Figure 4b is consistent with a hollow structure and shows that the shell is comprised of smaller nanoparticles. High-resolution TEM micrographs show randomly oriented nanocrystals in the shell, indicating that oriented attachment does not occur in this system. Elemental mapping data for a single sphere (Figure 4c) indicate that the hollow spheres contain both Co and

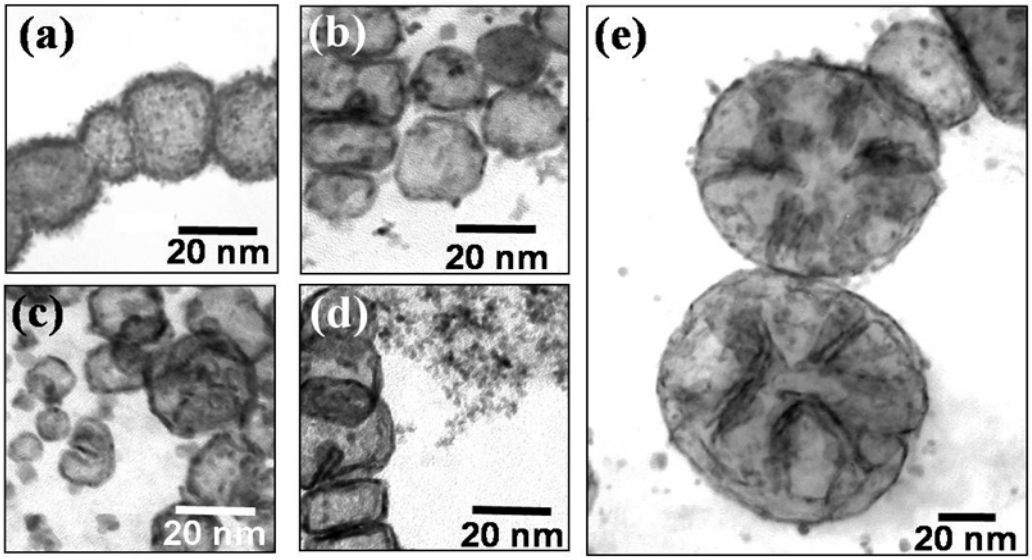

Figure 2. Hollow CoPt hollow spheres synthesized with varying stoichiometric ratios of Co:Pt. Particles with (a) 1:1 stoichiometric ratio, (b) 2:1 stoichiometric ratio, (c) 3:1 stoichiometric ratio, (d) 4:1 stoichiometric ratio, and (e) enlarged view of Co/Pt hollow spheres using a 3:1 stoichiometry.

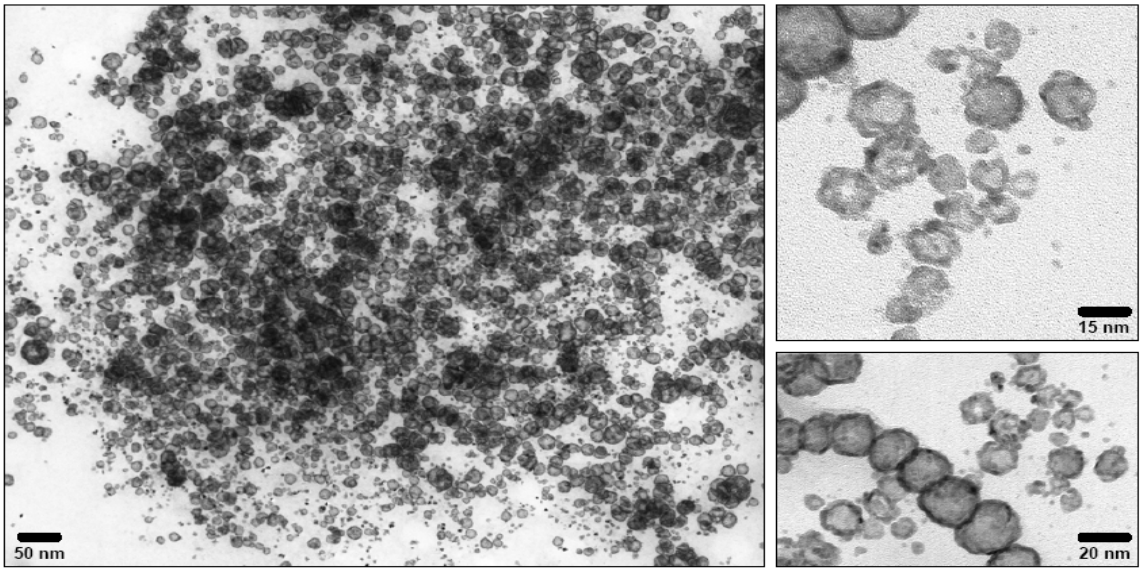

Figure 3. TEM images of $Co_{50}Pt_{50}$ hollow spheres. Some particles appear to be cracked during the reaction (top, right) and chains of particles are observed due to magnetic interactions between the spheres (bottom, right).

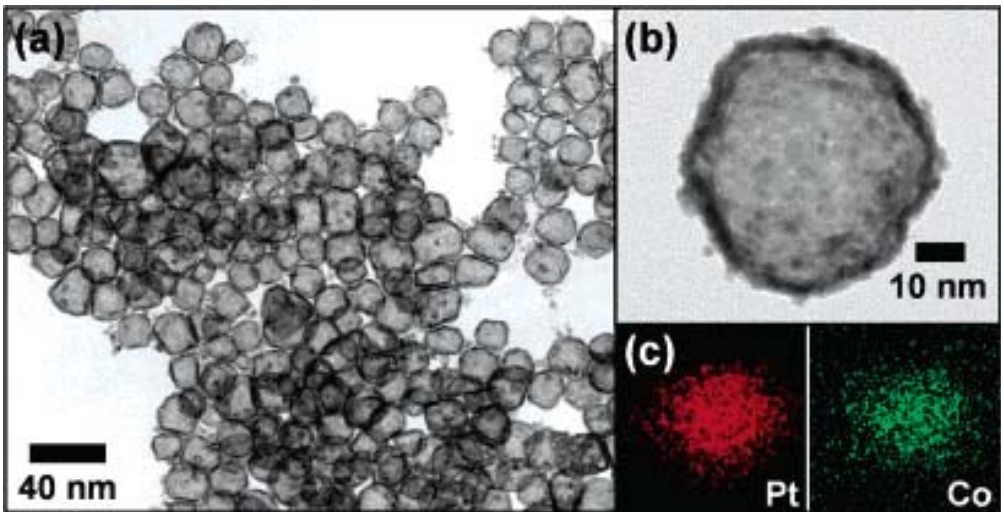

Figure 4. TEM micrographs of (a) CoPt hollow spheres and (b) a single hollow sphere showing that it is comprised of smaller particles; (c) elemental mapping data (Co and Pt) for the sphere in (b).

Pt. Energy-dispersive X-ray spectroscopy (EDS) data for many spheres confirm an average stoichiometry of $Co_{58}Pt_{42}$ (Figure 5a), and selected area electron diffraction (SAED) patterns show a single-phase fcc structure (Figure 5a, inset). Powder X-ray diffraction (XRD) data are also consistent with a single- phase fcc structure (Figure 5b). Importantly, the lattice constant for the fcc-type CoPt phase is a = 3.88 Å, which is measurably smaller than that of pure Pt (a_{lit} = 3.92 Å).

Taken together, the TEM, EDS, SAED, and XRD data are all consistent with the formation of hollow nanospheres with a CoPt alloy structure. This is further confirmed by XPS measurements (Figure 5c), which show that the Pt $4f_{7/2}$ peak is at 71.8 eV, compared to 71.2 eV that is expected for pure Pt. (The Pt 4f peaks are known to shift to higher energies upon alloy formation with Co.[116] The broad peaks in the XRD pattern in

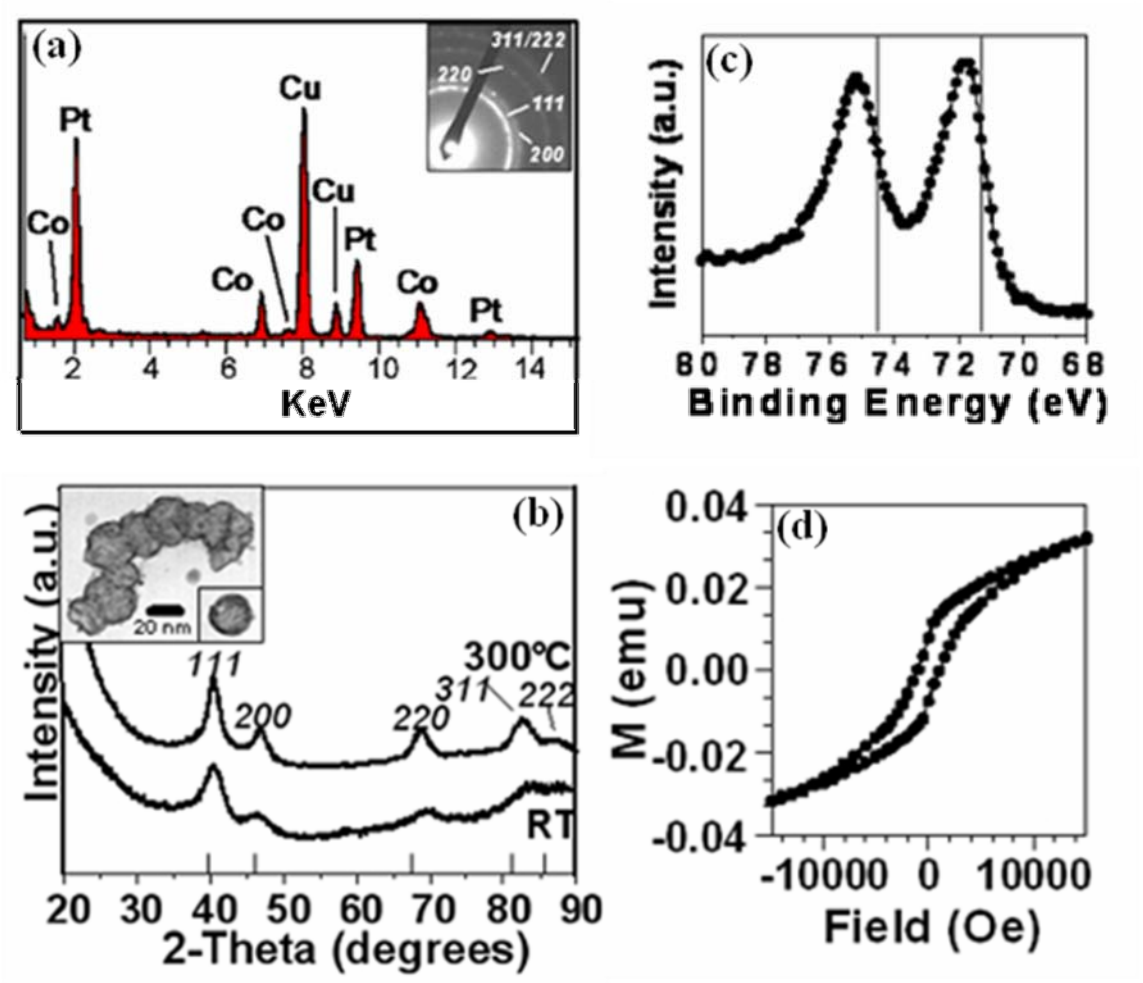

Figure 5. (a) EDS data and SAED pattern (inset) for CoPt hollow spheres (Cu is from the TEM grid); (b) XRD data for hollow CoPt nanospheres as synthesized at room temperature (RT) and after heating to 300 °C, showing shifting relative to the peak positions for Pt (tick marks), inset CoPt hollow spheres heated at 300 °C on a TEM grid; (c) XPS data for the Pt 4f peaks of CoPt hollow nanospheres (vertical lines show the $4f_{5/2}$ and $4f_{7/2}$ peak positions for Pt); (d) hysteresis loop at 5 K for hollow CoPt nanospheres.

Figure 5b are also consistent with the nanocrystalline nature of the shell, yielding an average particle size of 5 nm based on analysis using the Scherrer equation.

The TEM images in Figure 6a-c provide insight into the formation mechanism of the hollow CoPt nanospheres. Figure 6a shows a TEM micrograph of Co nanospheres that were isolated after $NaBH_4$ was added to the solution of Co^{2+} and PVP (before Pt^{4+} was added), suggesting that these dense spheres provide an in situ template for the

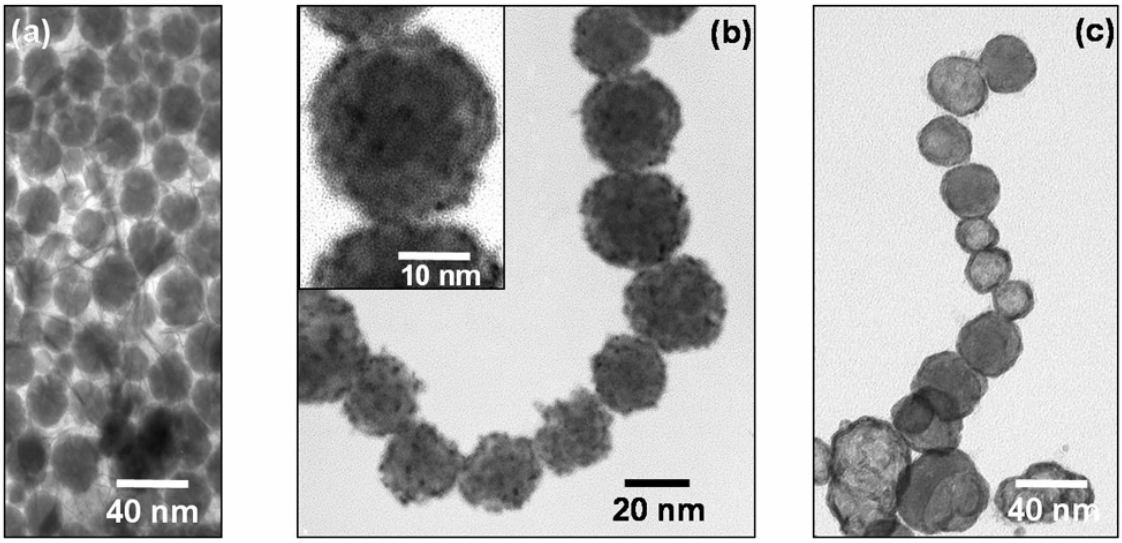

Figure 6. (a) Co nanoparticle template generated in situ and CoPt samples taken after reaction times of (b) 1 min and (c) 5 min.

formation of the hollow CoPt spheres. The TEM micrographs in Figure 6b, c correspond to samples reacted for 1 and 5 min, respectively. The spheres in Figure 6b are mostly dense, but a hollow region between the shell and the core is evident (Figure 6b, inset). This is consistent with a replacement reaction, where the Co core is sacrificially dissolved as the Pt shell is deposited. The standard reduction potentials for the Co^{2+}/Co [$E°$ = -0.277 eV vs standard hydrogen electrode (SHE)] and $PtCl_6^{2-}/Pt$ [$E°$ = 0.735 eV vs

SHE] redox pairs support this hypothesis. Very few nanospheres that simultaneously show well-defined core, hollow, and shell regions (Figure 6b) were observed. In most cases, the nanospheres were either dense or hollow (Figure 6c), suggesting that once an individual Co sphere begins to react with Pt^{4+}, the reaction goes to completion very quickly. The hollow spheres are thermally stable up to 300 °C when immobilized on a TEM grid (Figure 5b, inset) and maintain the CoPt alloy structure (Figure 5b).

While there are several reports of hollow sphere formation via galvanic displacement reactions,[55,56,95] there are no examples where Co-based alloys form as the final products when Co nanoparticles are used as templates.[99,107] We believe that the formation of hollow CoPt alloy nanospheres, which is a significant result, is directly related to the synthetic details involved in the one-pot reaction. There is excess BH_4^- in the reaction flask, so any Co that is oxidized to Co^{2+} during Pt deposition will be reduced back to Co. At the same time, PVP is present as the surface stabilizer, and its long polymeric chain structure will completely surround one or more nanospheres. Since PVP is known to bind metal cations,[117] it can trap the Co^{2+} that is liberated during the galvanic displacement reaction and allow it to combine with Pt^{4+} and co-reduce near the surface of the template nanosphere. The result is a shell that contains both Co and Pt in the form of an alloy. Previous reports of Pt, Au, and Au-Pt hollow nanospheres formed via Co nanoparticle templates use *molecular* stabilizers, such as citric acid, and always yield hollow spheres containing no Co.[99,107]

Measurements of magnetization versus applied field, obtained using a SQUID magnetometer, showed hysteresis at 5 K (Figure 5d) with a coercivity of 980 Oe,

indicating ferromagnetism. The significant paramagnetic background and lack of saturation is likely a result of impurity phases, such as cobalt oxides, or the dispersity in size and particle-particle separation of the constituent nanoparticles. Higher-temperature magnetic measurements indicate superparamagnetism, which is consistent with the small size of the individual nanoparticles that comprise the hollow nanostructures. The successful synthesis of hollow nanospheres of a CoPt alloy phase had several important implications since hollow alloy systems have received much less synthetic development than single-metal systems.

This work describes a straightforward way to access hollow alloy nanostructures and, as such, was extended to the NiPt (Figure 7), CuPt, and PbPt systems. Figure 7a shows XRD patterns of as-synthesized NiPt hollow particles in H_2O. The room temperature XRD pattern is shifted from that expected for pure Pt. Upon heating to 200 °C and 400 °C more Ni is incorporated into the shell and shifting in the peaks is observed in the XRD pattern. NiPt nanospheres appear to be comprised of smaller nanoparticles but unlike the CoPt system, the yield of the smaller particles is higher than the hollow particles. This was more pronounced in the case for CuPt nanoparticles and XRD experiments showed no evidence that alloys were formed in this system. In the PbPt system, hollow spheres were formed when synthesized in H_2O. However, XRD patterns did not show unambiguous evidence for the formation of alloys. Several experiments were performed in which the mole ratio of reactants, M:Pt (M = Co, Cu, and Pb), was varied by intervals of 1/8 until a reaching a 4:1 stoichiometry. The yield

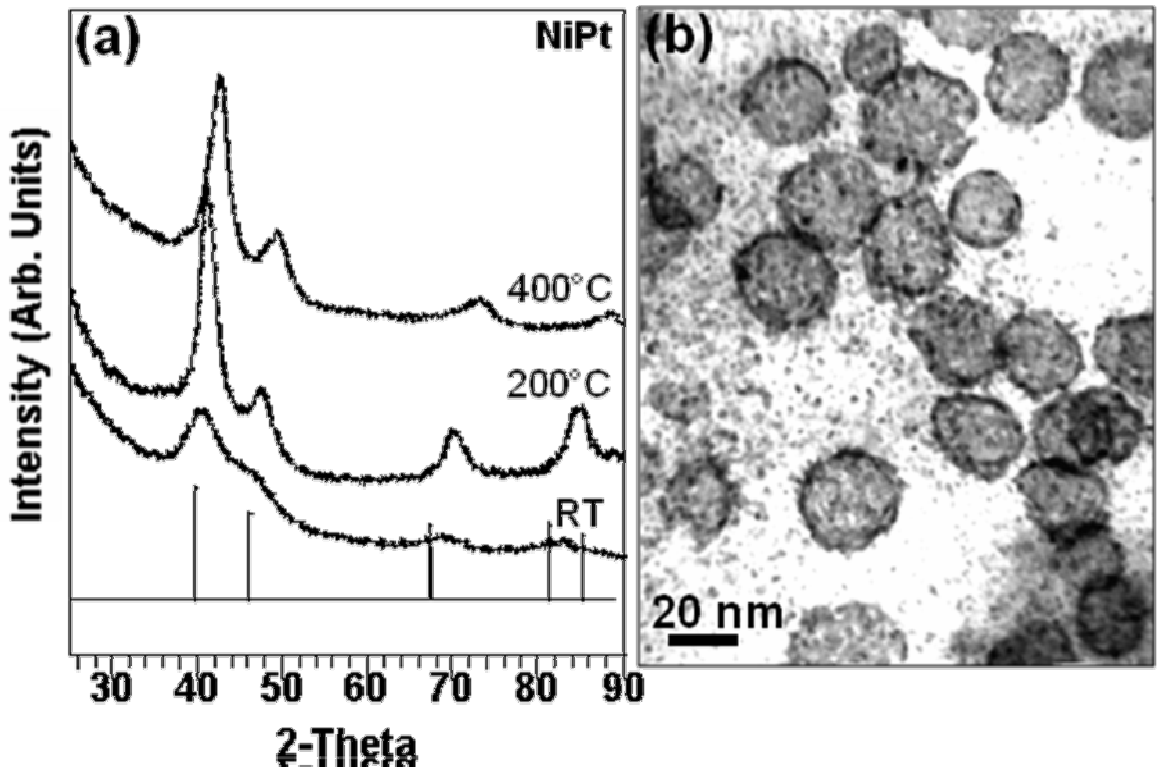

Figure 7. (a) XRD pattern of NiPt hollow spheres as synthesized in H_2O at RT. The RT samples were heated to 200°C, and 400°C in a tube furnace (Pt XRD pattern included as a reference (bottom)); (b) TEM micrograph of NiPt hollow particles.

of the hollow particles did not improve. Varying the temperature of the reaction from 0°C to 100°C in the PbPt system resulted in the formation of the mineral Hydrocerrusite which was an impurity present in some of the samples because of the ambient humidity.

From the work with CoPt, we hypothesized that the size, shape, degree of hollowing, and composition of the particles could be controlled such that shape controlled intermetallic shells could be synthesized in organic solvents. The next section describes our synthetic attempts at this aim.

Synthesis of PbPt intermetallic hollow spheres

Magnetic and superparamagnetic hollow spheres such as alloyed CoPt are of great interest for their potential applications as drug delivery vehicles and for separations in heterogeneous catalysis. Intermetallic hollow spheres could also have applications in catalysis since intermetallic compounds are known to have enhanced catalytic activity compared to alloys.[78,115] Many important organic and fuel cell reactions are catalyzed by expensive precious metals such as Pt, Pd, and Au, which are not cost effective for large scale applications. Intermetallic hollow nanoparticles could be an effective solution to solve such a problem because nanoscale particles are known to have enhanced catalytic activity compared to bulk. The geometry of the atoms on the surface of intermetallic compounds often enhances the selectivity of the reaction it catalyses and decreasing the amount of precious metals needed to catalyze the reactions would lead to cost reduction.

Early experiments with water based reactions in the PbPt system resulted in hollow particles but the reactions were so quick that it was not possible to control the composition of the shell. By XRD, the particles were determined to be Pt, and we could not unambiguously determine whether alloyed particles formed by this method in this system. Intermetallics could not be formed at any temperature between RT and 100˚C in water. Hence, a higher boiling point solvent, TEG, was chosen. Figure 8 shows intermetallic PbPt particles synthesized in 50 and 20 mL of TEG at 120°C, the lowest temperature at which the intermetallic was formed using these reaction conditions. Reactions where Pb and Pt salts were co-reduced in 50 mL of TEG did not result in hollow spheres as a product and neither did the sequential addition of Pt followed by Pb.

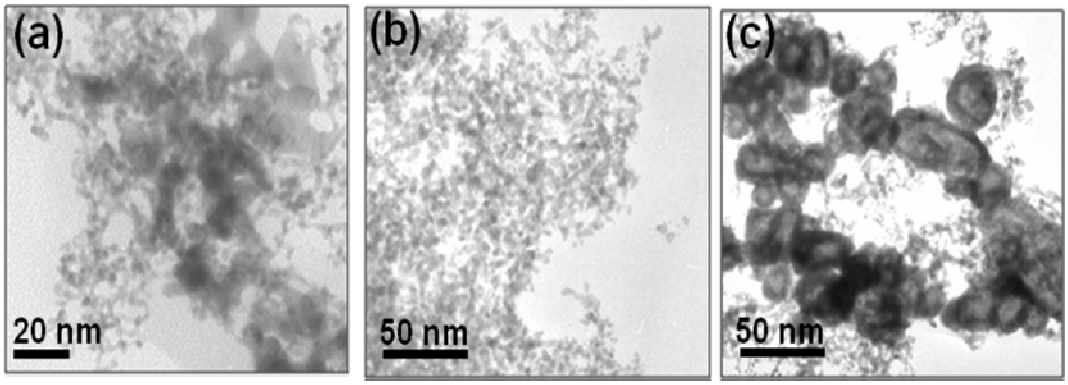

Figure 8. PbPt intermetallic nanoparticles synthesized in (a) 50 mL of TEG with sequential addition of $Pb(Ac)_2$ followed by solution of K_2PtCl_6. PbPt synthesized in (b) 20 mL of TEG by sequential addition of K_2PtCl_6 followed by $Pb(Ac)_2$, (c) 20 mL of TEG by sequential addition of $Pb(Ac)_2$ followed by K_2PtCl_6. All reactions were carried out in TEG at 120˚C with PVP (MW = 40, 000).

Hollow particles were observed when Pb was reduced first followed by reaction with the Pt salt in 20 mL of TEG at 120°C. However, the yield of hollow particles was very low (Figure 8c). In the previous section, Co nanoparticles in the 20-50 nm range appeared to form an in-situ template for the CoPt hollow particles. Based on these observations, we determined that hollow particles readily formed in this crucial size regime. Figure 8a and 8b most likely did not result in hollow particles because no Pb particles between 20-50 nm were formed under these reaction conditions to provide the in-situ template. In Figure 8c, some hollow nanoparticles in the 20-50 nm size regime were observed which further supports the idea that the size facilitates the formation of the hollow particles and also suggests that some Pb particles were formed in the 20-50 nm size regime. The size dependence in the synthesis of hollow particles has also been noted by other researchers.

In attempts to increase the particle size of the Pb particles to 20 nm or larger, higher temperatures were used, higher or lower molecular weight stabilizers were tested,

as well as varying the concentration of the reagents. Several experiments were performed at 120 °C, 140 °C, and 160 °C because these are temperatures at which the intermetallic compound formed; however, no hollow particles were observed and experiments at 220- 230 °C were undertaken since Xia and co-workers[118] had already shown that 100 nm discrete, spherical Pb colloids could be synthesized using PVP (MW = 55, 000) as the stabilizer in EG. Increasing the molecular weight of the stabilizer could lead to more discrete particles and not chains or networks of particles, but can also result in the formation of particles that are too small. The idea behind decreasing the molecular weight of the stabilizer (PVP, MW = 8,000) is that the resulting nanoparticles could be larger than the particles observed in Figure 8. Figure 9 is representative of several parameters tested to form the hollow PbPt nanopheres. When only 100 mg of PVP were used to synthesize the PbPt nanoparticles in TEG, the resulting nanoparticles were networked and agglomerated. In Figure 9a, 200 mg of PVP (MW = 40, 000) were used and resulted in larger particles that were still networked. When $NaBH_4$ was increased to 20 mg (doubled from 10 mg) (Figure 9b), the nanoparticles formed were not discrete and when PVP and $NaBH_4$ were both doubled, irregular shaped nanoparticles were formed (Figure 9c). Agglomerated clumps with some loose PbPt nanoparticles were the result of decreasing the amount of PVP (MW = 40, 000) to 50 mg (Figure 9c). In work by Chou and Schaak,[80,81] the Sn morphology was controlled using excess Sn and $NaBH_4$ to produce β-Sn nanorods which were subsequently converted hollow particles of PtSn. Along these lines, the stoichiometric amount of $Pb(Ac)_2$ was increased to a 2:1 Pb:Pt

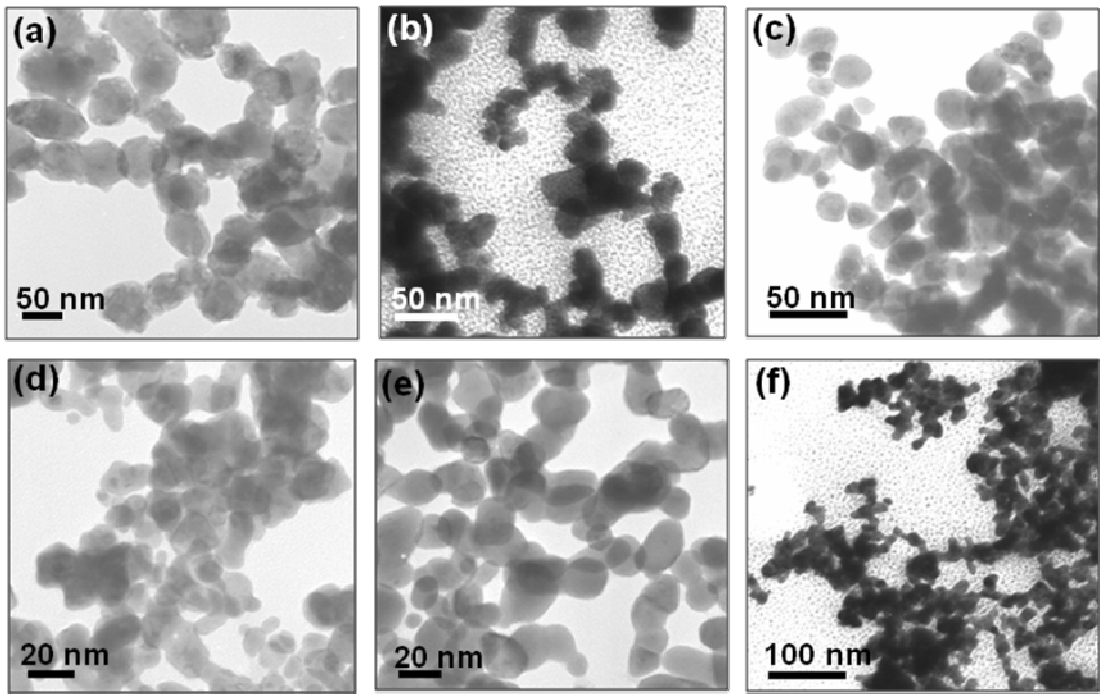

Figure 9. (a) Synthesis of PbPt nanoparticles with 200 mg of PVP. PbPt synthesized with (b) 20 mg of $NaBH_4$, (c) 20 mg of $NaBH_4$ and 200 mg of PVP, (d) 50 mg of PVP, (e) 20 mg of $NaBH_4$, 22 mg of $Pb(Ac)_2$ and 200 mg PVP, and (f) 100 mg of PVP (MW 8, 000). (PVP = 40,000 unless otherwise stated. Reactions were carried out at 230˚C.)

mol ratio, 200 mg of PVP, and 22 mg of $NaBH_4$, which gave PbPt nanoparticles in sizes between 20-30 nm and with a smooth surfaces, but they were not hollow (Figure 9e). Decreasing the molecular weight of PVP to 8, 000 resulted in highly networked particles (Figure 9f) similar to decreasing the amount of PVP (MW = 40, 000) to 50 mg. In all cases, the intermetallic NiAs structure was formed even when the Pb:Pt stoichiometric ratio was increased to 2:1. Sequential addition of the Pb precursor followed by the Pt precursor was done in all the cases described above and hollow particles were not formed. Because K_2PtCl_6 is not very soluble in TEG, $Pt(acac)_2$ was used as the Pt precursor, irregular shaped PbPt intermetallic nanoparticles formed with no hollow ones

evident by TEM (Figure 10a). Time allotted between the reduction of Pb and the addition of Pt was varied from 5 min to 3 h (Figure 10). Figure 10b shows that when Pt was added after 30 min, the particles formed clumps rather than discrete particles (the reaction conditions were the same as in the experimental section-PVP/$NaBH_4$/Pt source were not varied).

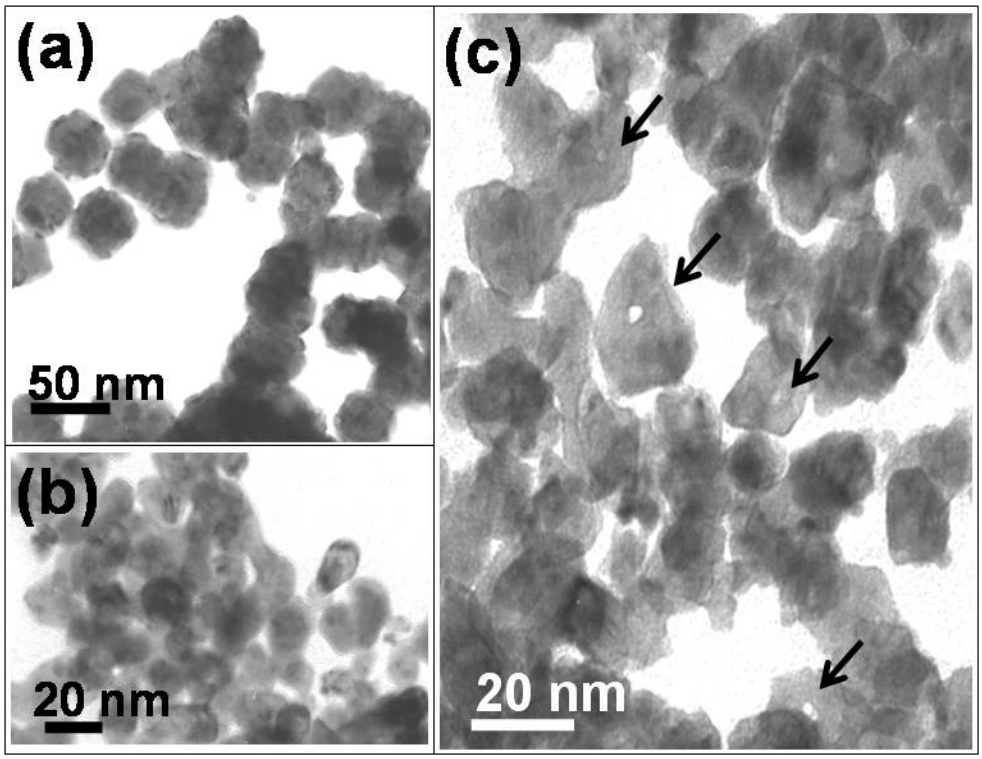

Figure 10. (a) PbPt nanoparticles synthesized at 120˚C using $Pt(acac)_2$ as the Pt source. PbPt particles synthesized by (b) addition of K_2PtCl_6 30 min after Pb reduced, (c) addition of K_2PtCl_6 3 h after $Pb(Ac)_2$ was reduced. Arrows indicate intermetallic PbPt hollow spheres.

Figure 10c shows some hollow particles formed when Pb was reduced and heated for 3 h before the Pt salt was injected into the hot 120˚C TEG/Pb solution. It is evident that these particles are in the critical 20 nm size regime. The main obstacle faced in synthesizing PbPt in TEG was that the nanoparticles had to be between 20-50 nm. Experiments where 50 mg of PVP and 50 mg of PEO were used to further stabilize the particles did not result in hollow spheres. Because Pb is a very low melting metal, the particles must be strongly stabilized otherwise the particles form networked nanoparticles which is what was observed in many of the samples synthesized in TEG.

Unlike CoPt, alloyed PbPt hollow particles could not be accessed in water. The product of the reaction of Pb nanoparticles with K_2PtCl_6 in water was hollow particles of Pt (Figure 11a) and most likely Pb_xO_y. When the Pt/Pb_xO_y composite was redispersed in 5 mL of TEG and heated to temperatures between 120°C and 160°C, hollow networks of the intermetallic NiAs type PbPt were formed (Figure 11b). The electron diffraction pattern (Figure 11c) and XRD pattern are consistent with NiAs type PbPt (Figure 11d). No direct evidence of Pb_xO_y was seen by XRD, but was probably present as amorphous Pb_xO_y (Figure 11d). There is no significant shifting in the XRD peaks that would indicate that alloys were formed for the hollow particles synthesized in water (Figure 11d).

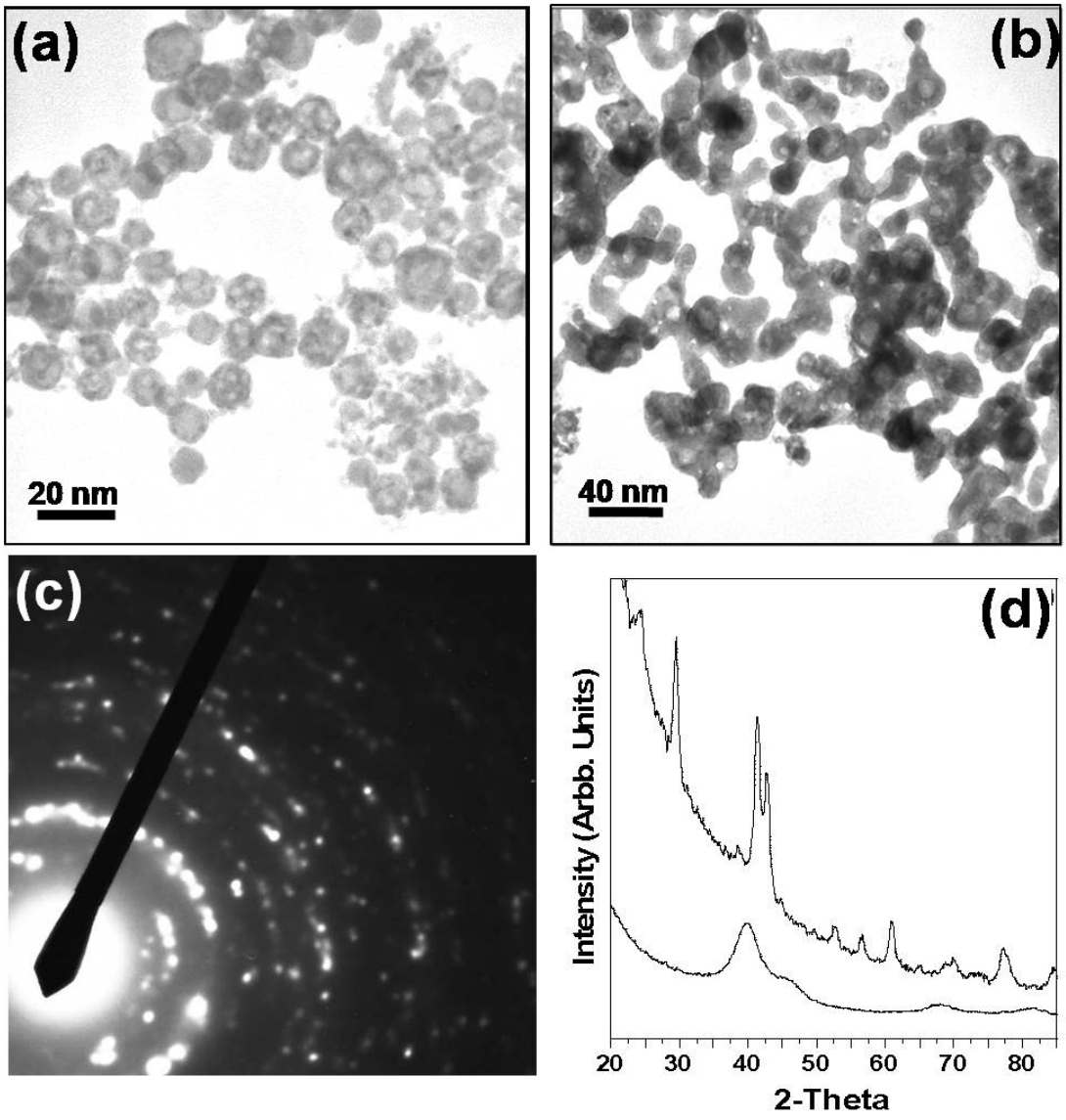

Figure 11. (a) Pt hollow particles synthesized in Nanopure water using Pb as the morphological template. (b) NiAs structure PbPt nanoparticles formed by heating particles in (a) at 120°C in TEG; (c) ED of intermetallic PbPt nanoparticles formed by heating hollow Pt nanoparticles and Pb_xO_y in TEG, (d) XRD pattern of hollow Pt nanoparticles (bottom pattern) and intermetallic PbPt (top pattern).

CONCLUSION

CoPt and NiPt alloys could be readily synthesized in water. PbPt formed a composite of Pt hollow particles with Pb_xO_y that when heated above 120 °C in TEG yielded hollow intermetallic PbPt (NiAs-type structure) nanocrystals. In these examples, metal nanocrystals (i.e. Co, Ni, and Pb) serve as in situ templates for the synthesis of hollow single metal, alloy, and intermetallic nanocrystals. These morphologies cannot be accessed using more direct co-reduction methods. Hollow particles have important potential applications in drug delivery, catalysis, and as composite materials. In particular, there is interest in synthesizing high surface area alloy catalysts for fuel cell applications, and hollow intermetallic nanocrystals such as PbPt may be good targets for such studies.

CHAPTER III

LOW TEMPERATURE SOLUTION SYNTHESIS OF GOLD-BASED INTERMETALLICS*

INTRODUCTION

Alloys and intermetallic compounds of Au with the magnetic 3*d* elements Fe, Co, and Ni are fascinating materials because they are non-equilibrium phases that are of interest for their catalytic,[119] magnetic,[120-125] optic,[122,126] and magneto-optic properties.[126] For example, Au-Fe alloys exhibit spin glass behavior and chiral susceptibility,[124,125] as well as combined plasmonic and superparamagnetic properties as nanoparticles.[126] Despite the miscibility gap that exists between Au and the magnetic 3*d* elements, several methods have succeeded at preparing a variety of atomically-*disordered* Au-*M* (*M* = Fe, Co, Ni) alloys.[119-126] However, the atomically-*ordered* non-equilibrium Au-*M* intermetallics are often the subject of theoretical prediction[127-130] but, for the most part, remain elusive experimentally. $L1_0$-type AuFe has been artificially fabricated by depositing and annealing alternating monolayers of Au and Fe,[131] as well as by vacuum annealing of Au nanoparticles overgrown with Fe via evaporation.[132] Au-Ni and Au-Co intermetallics have occasionally been observed via interfacial diffusion, co-evaporation,

---

*Reprinted in part with permission from "Low-Temperature Solution Synthesis of the Non- Equilibrium Ordered Intermetallic Compounds Au_3Fe, Au_3Co, and Au_3Ni as Nanocrystals" by Vasquez, Y.; Luo, Z. P.; Schaak, R. E., 2008, *J. Am. Chem. Soc.*, 130, 11866-11867. Copyright [2008] by the American Chemical Society.

and ion beam manipulation.[133-136] To the best of our knowledge, there have been no reports of $L1_2$-type Au_3M intermetallic formed as isolatable solids. Here we report the synthesis of the ordered intermetallic compounds Au_3Fe, Au_3Co, and Au_3Ni with the $L1_2$ (Cu_3Au) structure as nanocrystals using low-temperature solution chemistry techniques. The synthetic strategy is mild compared to the conventional high-temperature routes and has the potential to be general to yield other non-equillibrium intermetallics.

EXPERIMENTAL SECTION

Chemicals. All chemicals were used as received. Octyl ether ($C_{16}H_{34}O$, Aldrich, 99%) was used as the solvent for all reactions. The following metal reagents were purchased from Alfa Aesar: $HAuCl_4 \cdot 3H_2O$ (99.99%), $Fe(C_5H_7O_2)_3$ [$Fe(acac)_3$, 100%], $Ni(C_5H_7O_2)_2$ [$Ni(acac)_2$, 99%], $Co(C_5H_7O_2)_2$ [$Co(acac)_2$, 100%], and 2.86 M n- butyllithium [$CH_3(CH_2)_3Li$] in hexanes. Oleylamine (70%) was purchased from Aldrich.

Characterization. Powder X-ray diffraction (XRD) data were collected on a Bruker GADDS three circle X-ray diffractometer using Cu Kα radiation. Transmission electron microscopy (TEM), selected area electron diffraction (SAED) patterns, nanobeam electron diffraction (NBED) patterns, and X-ray energy-dispersive (EDS) data were collected using a JEOL JEM-2010 TEM at 200 kV. NBED patterns were taken using a 10 nm beam. Samples were prepared by sonication of the metal nanoparticles in ethanol and drop coating onto a carbon-coated copper grid. MacTempas software was used to produce simulated electron diffraction patterns. NBED was the technique used to determine the structure of the nanoparticles since using SAED requires a large area of the specimen to contribute to the diffraction pattern and often results in the reduction of

features in the patterns.[137] NBED is a type of convergent beam electron diffraction (CBED) which allows one to use a small aperture to overcome the spatial resolution limitation of SAED. Unlike SAED, which uses a parallel beam to illuminate the sample, in CBED a convergent beam is used to obtain diffraction patterns that allows for patterns to be taken of areas as small as 10 nm depending on the camera length and the size of the C2 aperture.[137]

Synthesis of Fe_3Au, Co_3Au, and Ni_3Au intermetallics. The synthesis was modified from a procedure published by Zhou et al.[138] In a typical reaction to synthesize Fe_3Au nanoparticles, $HAuCl_4 \cdot 3H_2O$ (10.0 mg), oleylamine (50 μL), and the appropriate amount of $Fe(acac)_3$ to yield a 3:1 molar ratio were added to 5 mL of octyl ether and heated to 80 °C under Ar. Then, 0.7 mL of 2.81 M n-butyllithium was added quickly via syringe to 10 mL of octyl ether, also at 80 °C and under Ar. Finally, the 5-mL octyl ether metal salt solution at 80 °C was added quickly via syringe. The reaction mixture was heated to 250 °C, the heat was turned off, and the sample was cooled to room temperature. The product was isolated by adding 10 mL of ethanol, centrifuging at 13 krpm, then extracting into the toluene layer of a toluene/water mixture. Co_3Au nanoparticles were synthesized following a similar procedure to Fe_3Au, except $Co(acac)_2$ was used instead of $Fe(acac)_3$. Ni_3Au nanoparticles were synthesized following a similar procedure to Fe_3Au, except $Ni(acac)_2$ was used instead of $Fe(acac)_3$.

RESULTS AND DISCUSSION

The original idea of this work was that n-butyllithium would co-nucleate the metals as nanoparticles due to the fast co-reduction of the metal reagents by the strong reducing agent.[138] In order to find the appropriate conditions to form the intermetallic nanoparticles, experiments varying the stoichiometry of the reagents were performed. Figure 12 shows XRD data of different stoichiometric ratios used to synthesize the intermetallic nanoparticles in the Au/Co system. Alloys of Au/Co formed at stoichiometries of 1:2, while the intermetallic phase was formed at a 1:3 and 1:3.5

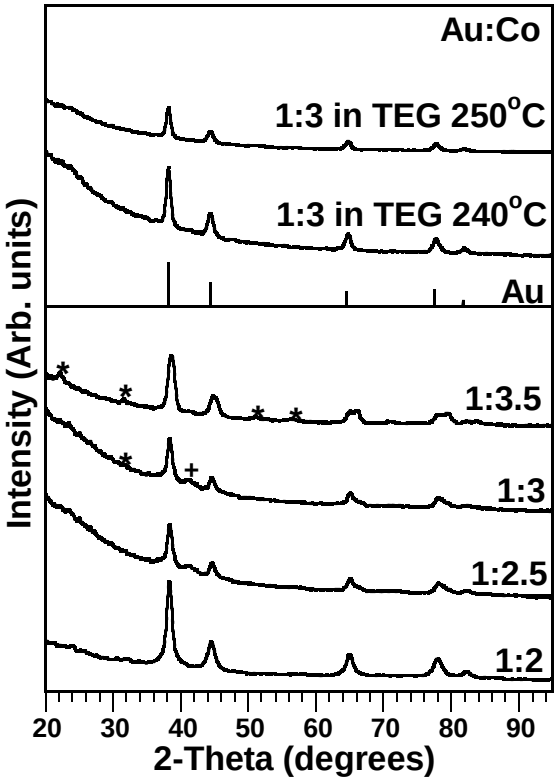

Figure 12. X-ray diffraction patterns for Au/Co products formed at 240°C at different stoichiometric ratios in octyl ether (bottom), and products formed using a 1:3 Au/Co stoichiometry in TEG at 240°C and 250°C without $NaBH_4$ (top). (Asterisk (*) denotes superlattice reflections while + denotes uncharacterized impurity. The Au pattern is included for comparison.

stoichiometry of Au/Co using n-BuLi and octyl ether. In order to confirm our hypothesis that the formation of the alloys and intermetallics was unique to the n-butyllithium technique, attempts to synthesize the $L1_2$ phases using common nanoparticle preparation protocols, such as the polyol method were performed. TEG was the solvent of choice in the polyol method and several parameters were tested such as varying the composition, temperature, and using $NaBH_4$ as a reducing agent, however, these attempts did not yield alloys or intermetallics in any of the *M*-Au systems and resulted in Au as the only product by XRD (Figure 12).

Figure 13 shows the powder XRD pattern for Au_3Fe using n BuLi as a reducing agent, which matches that expected for the cubic $L1_2$ structure. The lattice

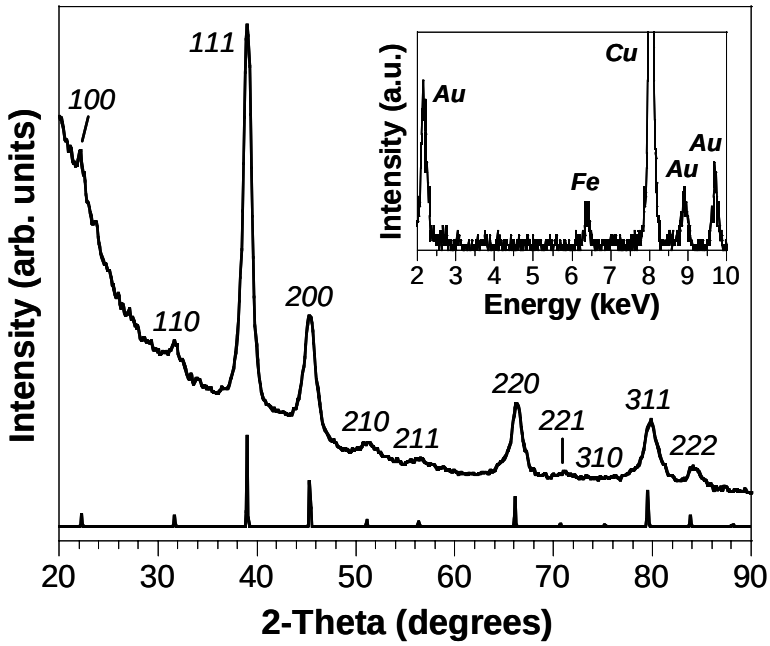

Figure 13. Experimental (top) and simulated (bottom) powder XRD patterns for $L1_2$-type Au_3Fe. Inset: EDS spectrum for Au_3Fe nanocrystals.

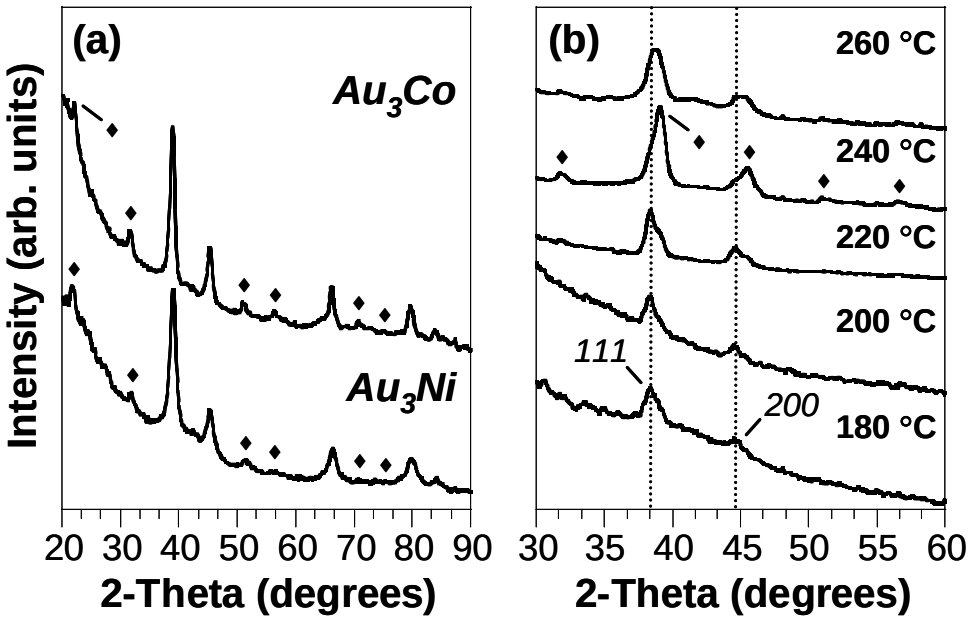

Figure 14. (a) Powder XRD data for Au_3Co and Au_3Ni. Diamonds (♦) indicate the $L1_2$ superlattice peaks. (b) Powder XRD data for aliquots taken during the synthesis of Au_3Co. Vertical lines correspond to the *111* and *200* peak positions for Au, and the diamonds (♦) denote the peaks corresponding to $L1_2$-type Au_3Co.

constant (a = 3.99 Å) is contracted relative to that of pure Au (a_{Au} = 4.08 Å), and the *100*, *110*, *210*, *211*, and *221* superlattice peaks characteristic of the $L1_2$ structure are clearly evident. Figure 14 shows the powder XRD data for Au_3Co (a = 4.00 Å) and Au_3Ni (a = 4.00 Å), which also have the expected $L1_2$ superlattice peaks. The Au-Co system provides insight into the reaction pathway that results in the formation of the non-equilibrium intermetallics. The original idea, as mentioned earlier, was that the rapid co-reduction of the metal reagents afforded by the strong reducing agent would allow them to effectively co-nucleate.[138] Figure 14b shows XRD data for aliquots taken during the formation of Au_3Co nanocrystals. At 180 °C, the crystalline product matches well with pure Au. Au is also the predominant product at 200 °C, with Au_3Co beginning to

appear by 220 °C. By 240 °C, the predominant product is Au_3Co. This shows that Au nucleates first, and the 3d transition metal reacts with the Au nanoparticles to form the Au_3M intermetallics. This is analogous to stepwise reaction pathways we have observed in the formation of other binary and ternary intermetallics using low-temperature solution routes.[30,77]

Interestingly, continued heating beyond 260 °C causes the superlattice peaks to disappear. This implies that the disordered alloy is the favored product and the ordered intermetallic is kinetically stabilized by low temperatures and short heating times. Attempts to form the Au_3M intermetallics using other common solution reduction techniques were unsuccessful in our hands, demonstrating that the reduction kinetics still play an important role in the reaction.

Figure 15 shows TEM micrographs and SAED patterns for the Au_3M nanocrystals. The Au_3Fe and Au_3Ni nanocrystals are generally spherical with an average particle size of around 20 nm, ranging from 15-30 nm throughout the sample. The Au_3Co nanocrystals are slightly larger with more elongation and faceting. High-resolution TEM micrographs of individual particles (Figure 15 and Figure 16) show that the nanocrystals are highly crystalline with lattice fringes of 2.3 Å, corresponding to the *111* plane of the Au_3M intermetallics. Figure 16 also shows that the particles are roughly spherical with some faceting occurring in the Au_3Fe system which results in hexagonal morphology. The electron diffraction patterns shown in Figure 15 also confirm the formation of the $L1_2$-type intermetallics, with the *100*, *110*, *210*, *211*, and *221* superlattice reflections clearly evident.

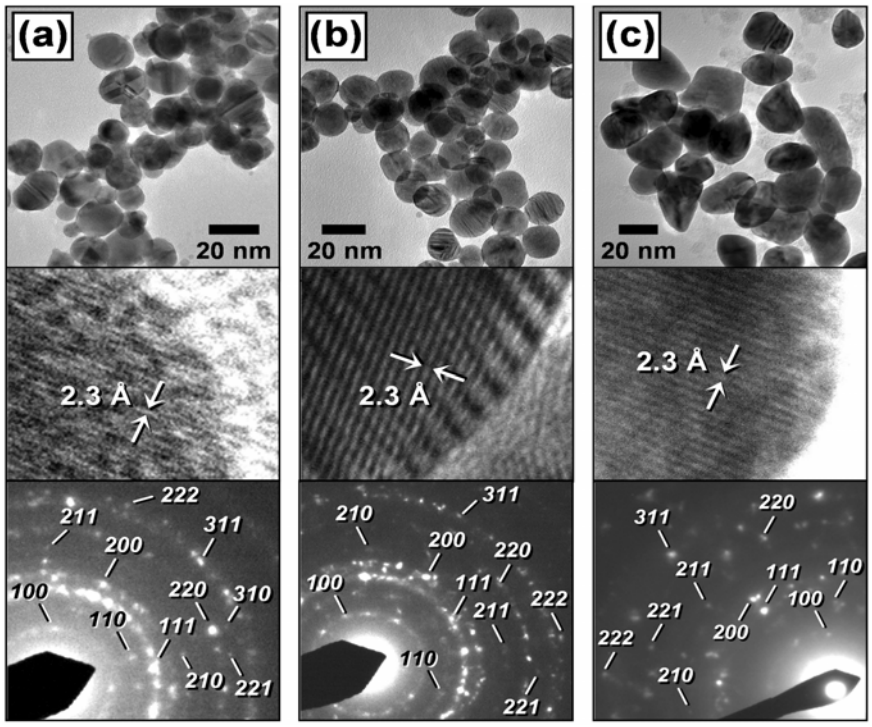

Figure 15. TEM images, high-resolution TEM images showing *111* lattice fringes, and electron diffraction patterns for $L1_2$-type (a) Au_3Fe, (b) Au_3Ni, and (c) Au_3Co nanocrystals.

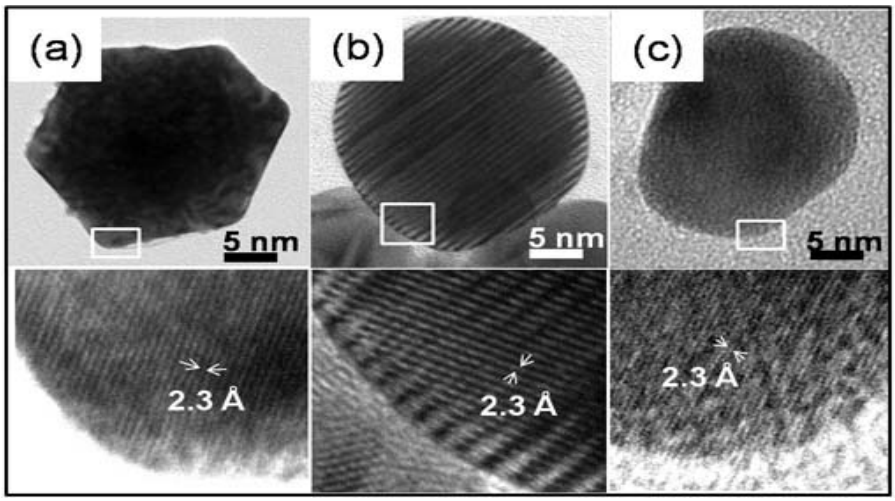

Figure 16. TEM micrographs and high resolution TEM micrographs of individual (a) Au_3Fe, (b) Au_3Ni, and (c) Au_3Co nanoparticles, showing the lattice fringes for the *111* planes. The boxes in the left-hand panels show the regions enlarged in the top panels.

The EDS data for Au_3Fe (Figure 13) indicate a 3:1 ratio for Au:Fe. All of the data are consistent with a bulk sample of Au_3M nanocrystals that crystallize in the ordered $L1_2$-type intermetallic structure. Nanobeam electron diffraction (NBED) patterns provide additional evidence for the formation of the Au_3M intermetallics. The NBED patterns were taken using a beam size of 10 nm in diameter on single isolated nanoparticles that were confirmed by EDS to have a stoichiometry of Au_3M (Figures 17 and 18).

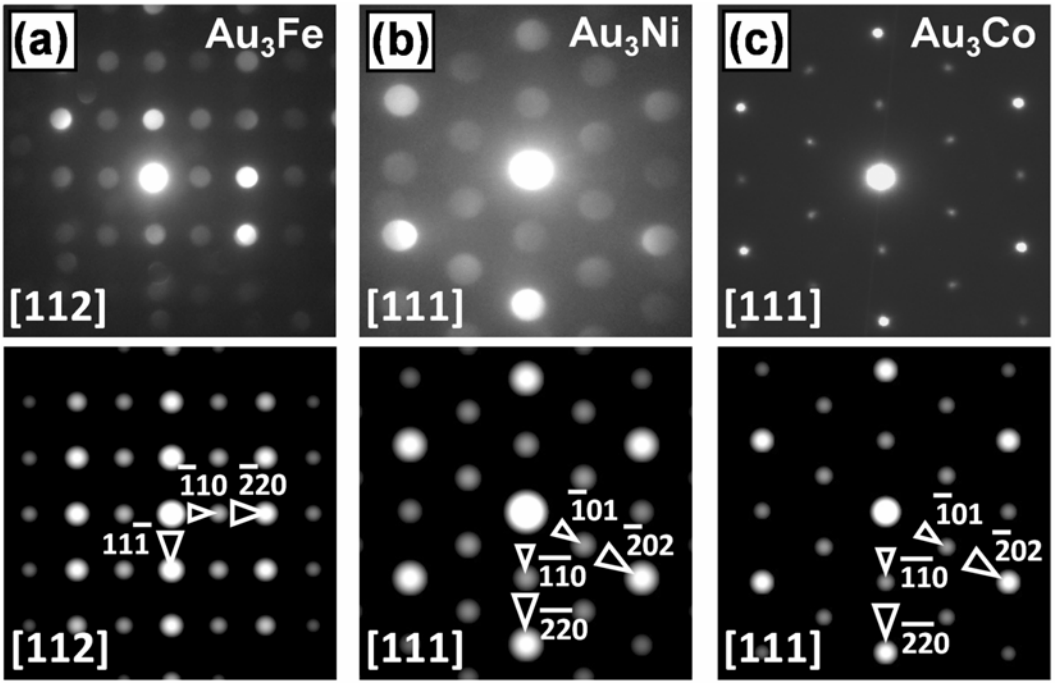

Figure 17. Nanobeam electron diffraction (NBED) patterns for individual nanocrystals of (a) Au_3Fe along the [112] zone axis and (b) Au_3Ni along the [111] zone axis. Selected-area electron diffraction pattern for a single Au_3Co nanocrystal along the [111] zone axis is shown in (c). Top: experimental; bottom: simulated.

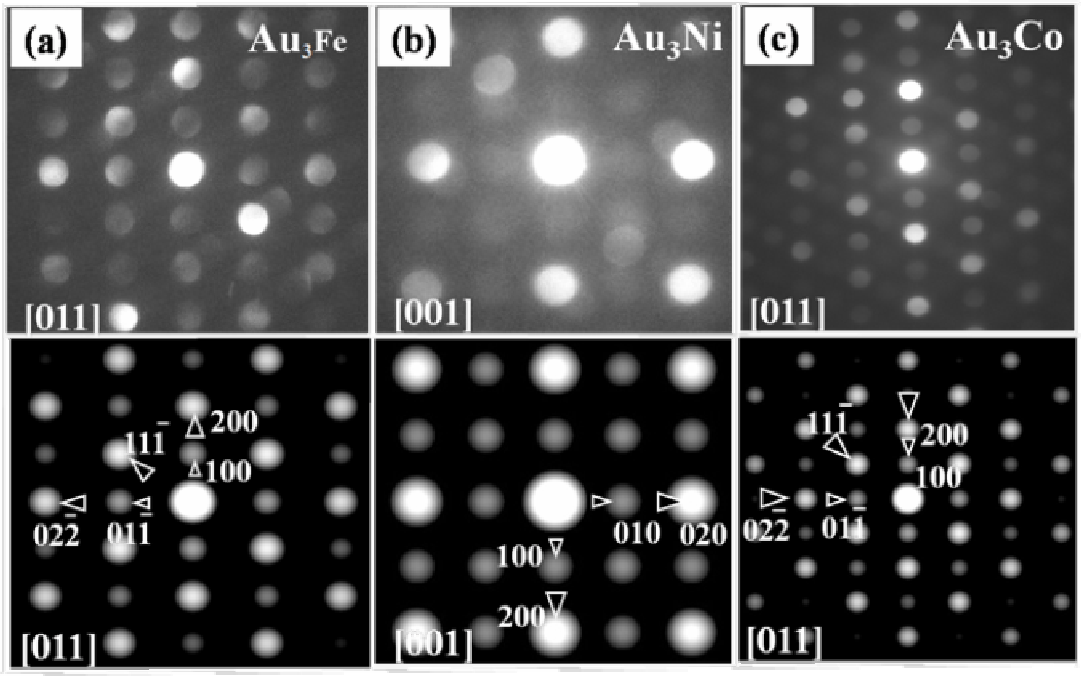

Figure 18. Nanobeam elecron diffraction (NBED) patterns for (a) Au_3Fe along the [011] zone axis, (b) Au_3Ni along the [001] zone axis, and (c) Au_3Co along the [011] zone axis. Top panels: experimental. Bottom panels: simulated. Large arrowheads indicate fundamental fcc reflections while small arrowheads indicate the superlattice reflections due to ordering.

Figures 17a and 17b show the NBED patterns from single Au_3Fe and Au_3Ni nanocrystals along the [112] and [111] zone axes, respectively. The strong reflection spots are from the fundamental fcc lattice (larger arrowheads, space group *Fm*-3*m*) while the weak superlattice reflections (smaller arrowheads) appear at the half positions of the fundamental reflections. This implies a primitive structure, consistent with the $L1_2$ superstructure (space group *Pm*-3*m*). Simulations using $L1_2$-type Au_3Fe and Au_3Ni as a model (Figures 17a and 17b) are consistent with the experimental patterns and further support the formation of $L1_2$-type nanocrystals. The slightly asymmetric intensity distribution of the NBED patterns is due to a small specimen tilt, and some extra spots

are from surrounding particles. Figure 17c shows a selected area electron diffraction (SAED) pattern collected along the [111] zone axis of a single Au_3Co nanocrystal (Figure 17c). This pattern, which is indicative of a single-domain particle, shows a strong contrast between the fundamental fcc lattice reflections and the superlattice reflections at the half positions. Figure 18 also shows more NBED patterns for the $L1_2$ intermetallics. These patterns also correspond to a primitive space group $Pm\text{-}3m$. Reflections along the [011] direction for both Au_3Fe and Au_3Co are slightly asymmetrical due to specimen tilt but weaker intensity is still evident for the superlattice reflections (small arrows) with the strong reflection spots clearly visible (large arrows). NBED patterns can be indexed and correspond well with the Cu_3Au prototype structure. The experimental data are consistent with the simulated data, providing additional evidence for the proposed $L1_2$ structure.

Figure 19 shows UV-Vis data for Au_3Co nanoparticles dispersed in ethanol. The absorption at 280 nm is attributed to cobalt oxide impurities and the peak around 520 nm is attributed to Au. While this sample did form the $L1_2$ structure, we do not definitively attribute any of the features in the UV-Vis data to the $L1_2$ structure. Because of magnetic interactions the nanoparticles could not be dispersed well in ethanol and clumped or precipitated out of the cloudy solution. Several solvents were used including hexanes, water, THF, toluene, and chloroform but the nanoparticles dispersed the best in ethanol.

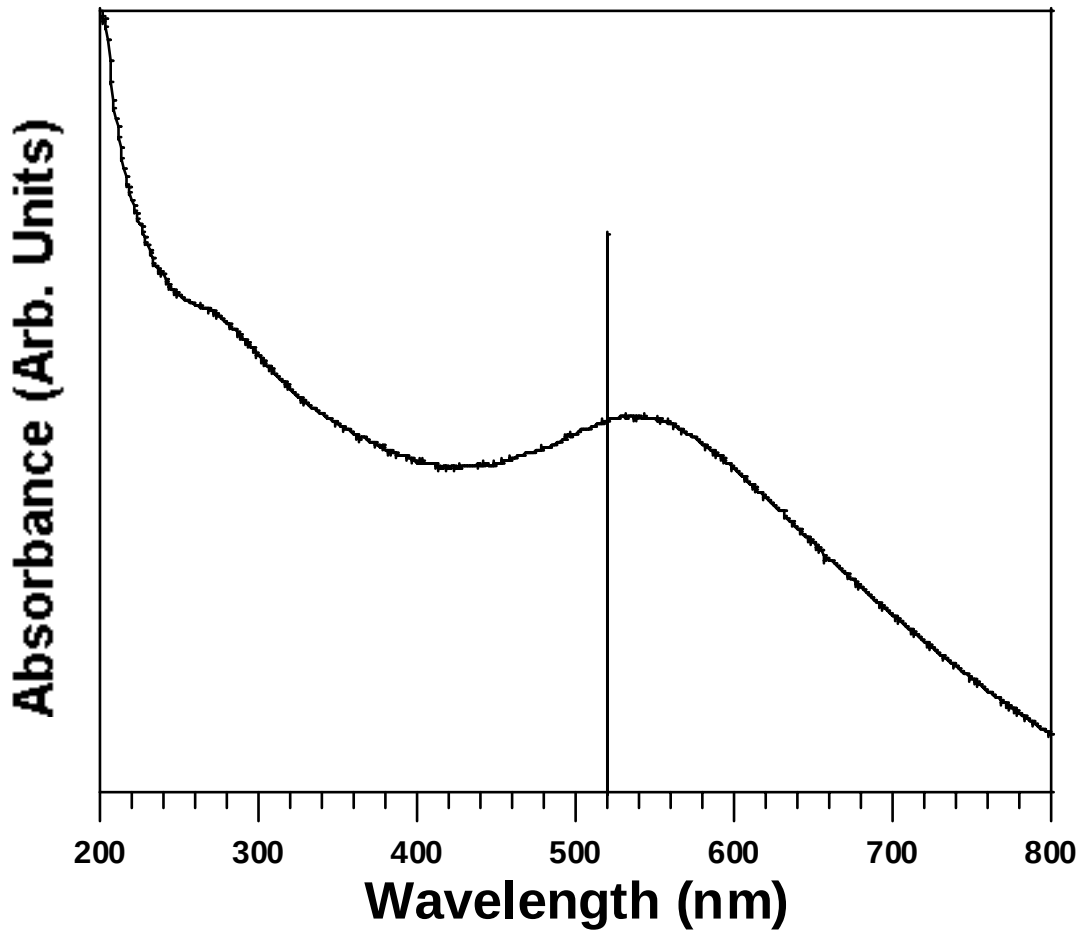

Figure 19. UV-Vis of Au_3Co in ethanol.

The Au_3M nanocrystal samples have small amounts of Au and MO_x impurities that complicate property measurements, and we cannot rule out the possibility that small amounts of impurities help to stabilize the $L1_2$ structure. However, the formation of the Au_3M ordered intermetallics is a significant result, since these non-equilibrium phases have been elusive, yet of interest for their magnetic, optical, and catalytic properties.

CONCLUSION

We have demonstrated a low temperature solution route for the synthesis of non-equilibrium intermetallics Au_3Fe, Au_3Ni, and Au_3Co. These intermetallics quickly disorder at temperatures above 260°C and are favored in a narrow temperature window between 240°C and 250°C, which implies that the ordered intermetallics are kinetically stabilized by low temperatures and short heating times. This synthetic route could potentially yield more non-equilibrium intermetallics.

CHAPTER IV

COMPOSITIONAL VARIANCE IN NANOCRYSTALLINE INTERMETALLIC COMPOUNDS SYNTHESIZED BY THE POLYOL METHOD

INTRODUCTION

The synthesis of nanoparticles has been driven by the challenge to find materials with new or improved properties. When solids are confined to the nanometer size regime, new structures can be stabilized,[80] meta-stable structures have been discovered,[76] or known structures with composition ranges not found in bulk have been observed. For example, α-$CoSn_3$ and $RuSn_2$ have been synthesized in tetraethylene glycol (TEG) at temperatures below 290°C.[80,81] As mentioned in Chapter I, bulk $CoSn_3$ is synthesized through a peritectic reaction or from Sn flux[82,83] and $RuSn_2$ has been reported as a metastable phase, but these phases can be easily synthesized as nanoparticles in solution. In some cases, the phenomena of stability in nanoparticles has been attributed to enhanced solubility in alloys[139] and, in others, it has been attributed to large surface energy or surface segregation. However, there still exist questions about the thermodynamics of nanoparticles and researchers are working to describe how variables such as surface energy, composition, pressure, shape, and size affect the equilibrium states or phase diagrams of nanoparticles.[140,141]

In bimetallic nanoparticles, the structure of the nanoparticle and the composition can be size dependent. As a new crystal nucleates, the depletion of a surrounding phase could occur given that there may not be enough of one of the components to construct

"critical" nuclei. Depending on the temperature, there may be a statistical distribution of particles in a single phase state and those in two phase states, i.e. in a single nanoparticle sample, there may be significant deviation in composition in the nanoparticles and different crystal structures may be also be present.[141] This variance in the composition and crystal structures is important to understanding the structure/reactivity relationships of bimetallic nanoparticles that may have useful applications in technology. Studying the size dependence, the composition, and crystal phases could also lead to a better understanding of nanoparticle phase diagrams. For example, Hills et al. use scanning transmission electron microscopy (STEM) to correlate the size, structure, and composition of Pt-Ru bimetallic nanoparticles.[142] Based on these studies, a phase diagram based on size and atomic % composition (size was substituted for temperature) was developed for Pt-Ru where it was found that several clusters are present in compositions that are metastable and not found in bulk. The particles had a wide composition range as alloys and 2-6 nm diameter particles were predominately present in the fcc structure although some nanoparticles (5-6 nm) were found with the hcp structure at 50% Ru.[142]

Similarly, in this chapter, we use transmission electron microscopy (TEM) to determine whether the composition varies from one particle to another in $AuCu_3$ and PtSn nanoparticles synthesized by the modified polyol method. $AuCu_3$ and PtSn systems were chosen for this study because they are prototypical "umbrella" and line phases. Both of these systems have been shown to be catalytically active and the variance in composition may affect the efficiency of the reactions they catalyze significantly. In

particular, the Au-Cu system is interesting to study since it is a well understood binary phase diagram with distinct intermetallic phases. The three structures AuCu, $AuCu_3$, and an extended structure are textbook models of order/disorder phase transitions and several experimental[143,144] and theoretical studies[145-147] have been published concerning ordering temperature, atomic distribution,[146] as well as theoretical calculations that predict phase/structure stability.[146,147]

In order to obtain data on the composition of these nanoparticles, electron microscopy was used, most notably scanning transmission electron microscopy (STEM), which is an extremely powerful tool to characterize small metal nanoparticles. STEM images would help to determine whether the nanoparticles are homogeneous and whether there is phase separation in both the $AuCu_3$ and PtSn. This is important to understanding whether significant deviations in the PtSn stoichiometry could be tolerated or if a $PtSn/SnO_2$ phase separation would result. Energy dispersive x-ray spectroscopy (EDS) was also used to determine the stoichiometry of individual nanoparticles within 5 atomic % percent, which is the instrumental error introduced by technique. This information is used to probe whether $AuCu_3$ and PtSn deviate in composition from their bulk phase diagrams.

As already mentioned, the size dependence and composition could help to formulate a phase diagram for these nanoparticles. However, what was found in this study is that the synthesis of $AuCu_3$ and PtSn by the modified polyol process hindered the STEM/EDS analysis due to instability of the samples under the TEM beam and was attributed to the inability to remove the thick polymer (PVP) coatings on the surface of

the nanoparticles that resulted from using PVP as the surface stabilizer in the synthesis. Unlike the study by Hills et al,[142] data on the size of the nanoparticles was not considered in these studies although it is an important parameter. The reason for this was that the size of the nanoparticles varied significantly with single particles, agglomerated nanoparticles, and networks of nanoparticles observed by TEM. Single particle EDS data could not be obtained for PtSn specimens due to beam instability, however, EDS data was gathered for large areas of PtSn nanoparticles within the viewing range. In the $AuCu_3$ specimen, EDS experiments were performed on 17 single $AuCu_3$ nanoparticles using both an FEI Tecnai G2 F20 and JEOL 2010F. Although the sizes were not accounted for in this study, EDS and STEM-mapping experiments should still give insight into the differences in compositions in both the PtSn and the $AuCu_3$ systems.

EXPERIMENTAL SECTION

Materials. The following metal reagents were used: $SnCl_2$ (anhydrous, 99% min.), $Cu(C_2H_3O_2)_2{\cdot}H_2O$ (98.0-102.0%), $HAuCl_4{\cdot}3H_2O$, $NaBH_4$ (98%), poly(vinyl pyrrolidone) (PVP, MW = 4, 000; MW = 630, 000; MW = 55, 000), $H_2PtCl_6 \cdot 6H_2O$, $AgNO_3$, ethylene glycol (EG), and tetraethylene glycol (TEG, 99+%). All chemicals were purchased from Alfa Aesar.

Synthesis of $AuCu_3$. The particles were synthesized via the modified polyol process adopted from Sra et al.[148] $Cu(C_2H_3O_2)_2$ (6.8 mg), $HAuCl_4{\cdot}3H_2O$ (13.3 mg), and poly(vinylpyrrolidone) (PVP, MW = 630, 000; 100 mg) were dissolved in 50 mL of tetraethylene glycol (TEG) via sonication in an 100 mL Erlenmeyer flask. The solution was degassed under Ar for 20 min, followed by addition of 25 mL of freshly prepared

0.01 M $NaBH_4$ dissolved in TEG. The solution was heated to 305°C and held for 10 min. After the solution cooled to room temperature, the nanocrystals were isolated by centrifugation and washing several times in ethanol to remove excess PVP. Although the mole ratio used in the original study by Sra et al. used a 1:1 mol ratio and AuCu intermetallic was found to form within 300-310 °C, the phase obtained in this case is the $AuCu_3$ structure ($L1_2$) between 300-305 °C.

Synthesis of PtSn. The particles were synthesized via a modified polyol process adopted from Cable et al.[149] Briefly, in a 40 mL vial 87.2 mg of $SnCl_2$ were dissolved in 20 mL of TEG via sonication and magnetic stirring, followed by the addition of 53.3 mg of K_2PtCl_6 and 170 mg of PVP (MW 40, 000). The solution was vigorously stirred and degassed under Ar for 30 min. 25 mg of $NaBH_4$ freshly dissolved in 5 mL of TEG were added slowly. The salt solution immediately turns black upon reduction and is then heated to 250°C. Powders were precipitated from solution by centrifugation and were washed with ethanol. Variations on this procedure included the use of 170 mg of PVP MW = 630,000, decreasing the amount of PVP to 100 mg (MW = 40, 000 and MW = 630, 000), increasing the amount of TEG to 50 mL, and increasing the amount of PVP to 400 mg MW = 40, 000. A conversion chemistry pathway to access more discrete PtSn nanoparticles was also used. Two major reasons for modifying the reaction conditions was the lack of beam stability due to polymer and the inability to perform single particle Energy Dispersive X-ray Spectrocopy (EDS) experiments due to small particle size and/or agglomeration. A two step “conversion chemistry” procedure was used to make more discrete nanoparticles. Pt nanoparticles synthesized by the polyol method were

reacted with $SnCl_2$ and heated to 200°C. The Pt nanoparticles were synthesized using a procedure by Song et al. Briefly, 125 mg of PVP (MW = 55, 000) were dissolved via sonication in 3 mL of ethylene glycol (EG). Then, 48.7 mg of $H_2PtCl_6 \cdot 6H_2O$ were dissolved in 1.5 mL of EG. A solution of 2 mM of $AgNO_3$ in 10 mL of EG was prepared. After adding 0.5 μL of $AgNO_3$ to 2.5 mL of EG at 198°C, 94.0 μL of the PVP/EG solution and 47.0 μL of $H_2PtCl_6 \cdot 6H_2O$/EG solution were added to the 2.5 mL of EG every 30 sec. for 15 min. When both solutions added, the reaction was maintained at 200°C for 5 min and allowed to cool to room temperature. 24 mL of acetone were added to the reaction and then centrifuged at 5, 000 rpm. 8.4 mg of Pt nanoparticles were dispersed in 20 mL of TEG along with 4.3 mols of $SnCl_2$ (35.1 mg). The reaction was degassed under Ar and heated to 200°C for 45 min. The PtSn nanoparticles were centrifuged at 13, 000 rpm and washed with ethanol.

Characterization. Powder X-ray diffraction (XRD) data were collected on a Bruker GADDS three-circle X-ray diffractometer using Cu Kα radiation. Transmission electron microscopy (TEM) images, STEM-HAADF images and Scanning Tranmission Electron Microscopy (STEM-EDS), and were taken using an FEI Tecnai G2 F20 equipped with HAADF detector operated at 200 kV at Texas A & M University. TEM images and EDS for the $AuCu_3$ samples were also taken using a JEOL 2010F Transmission Electron Microscope equipped with Field Emission Gun (FEG) operated at 120 kV at the University of Texas. Samples were prepared by sonicating the nanocrystalline intermetallic powders in ethanol and dropping a small volume onto a carbon-coated nickel or copper grid. In some cases the grids were dipped into the ethanol/nanoparticle

dispersions. Some samples were plasma cleaned using a Fishione 150 Plasma Cleaner for 15 sec. PtSn samples on Formvar carbon coated Ni or Cu grids that were plasma cleaned were unstable. $AuCu_3$ nanoparticles were stable when dropped on a Ni holey carbon grid that had been plasma cleaned for 10 sec.

RESULTS AND DISCUSSION

Transmission electron microscopy of PtSn

PtSn intermetallic nanoparticles were routinely synthesized using the modified polyol method having the prototypical NiAs structure. The synthesis adopted by Cable et al.[149] resulted in networks and not discrete particles. Since single nanoparticles would best serve the purpose for this study, several variations on the synthesis of PtSn were attempted. Variations on this procedure included the use of 170 mg of PVP MW = 630,000, decreasing the amount of PVP to 100 mg (MW = 40, 000 and MW = 630, 000), increasing the amount of TEG to 50 mL, and increasing the amount of PVP to 400 mg MW = 40, 000. In attempts to synthesize more discrete nanoparticles, 630,000 molecular weight PVP was used; however, the nanoparticles were still agglomerated. Experiments where PVP was increased to 400 mg PVP MW = 40, 000 and the amount of TEG was increased were also performed to reduce agglomeration in the nanoparticles. Both of these cases resulted in clumps of small particles (2-3 nm) that were difficult to image and perform single particle EDS measurements due to image drift and beam instability. In all the cases, the amount of PVP coating the surface of the nanoparticles made the samples unstable under the beam at high magnifications. In attempts to obtain more stable samples, the reactions were carried out at 290°C. PVP decomposes at higher

temperatures so it would be likely that some of the polymer would be decomposed at these higher temperatures. At 290°C, the NiAs structure type for PtSn was obtained with no impurities visible by XRD. However, beam stability continued to be a problem for these samples.

While EDS experiments could not be performed on single particles, STEM data were acquired for areas with small clusters of hollow PtSn nanoparticles. A mixture of hollow and solid PtSn nanoparticles were synthesized using a two step "conversion" method in which PVP stabilized Pt nanoparticles were reacted with $SnCl_2$ to produce the PtSn intermetallic nanoparticles at 250°C. Figure 20 shows that the particles were discrete in this sample and some hollow particles were observed. A high angle annular dark field (HAADF) image of these square shaped hollow particles shows that the particles are homogeneous with no significant phase separation between Pt and Sn. The brighter areas in the STEM HAADF image correspond to differences in the height of the sample. X-ray diffraction data shows that the particles adopt the NiAs intermetallic structure. Although the specimen contains discrete particles of PtSn, the specimen was not stable enough to produce a clear STEM-HAADF image (Figure 20a), or for single particle EDS, STEM EDS data, or elemental maps. Figure 20c shows a drift corrected HAADF image of a different specimen of PtSn nanoparticles. This sample was synthesized using the method by Cable et al.[149] except 400 mg of PVP (MW = 40, 000) was used instead of 170 mg. The particles are very small and agglomerated. A drift corrected STEM HAADF image of this specimen shows that the particles are very homogeneous with brighter areas corresponding to differences in height in the specimen

(Figure 20c). The blurriness in the image is due to image drift. Figures 20d and 20e are elemental maps of the Pt L-shell and Sn L shell respectively. Both elements are present throughout the sample which shows no apparent evidence for phase separation in PtSn synthesized by the polyol method. However, because of image drift and instability, high resolution data were not collected and we cannot definitively rule out the possibility for

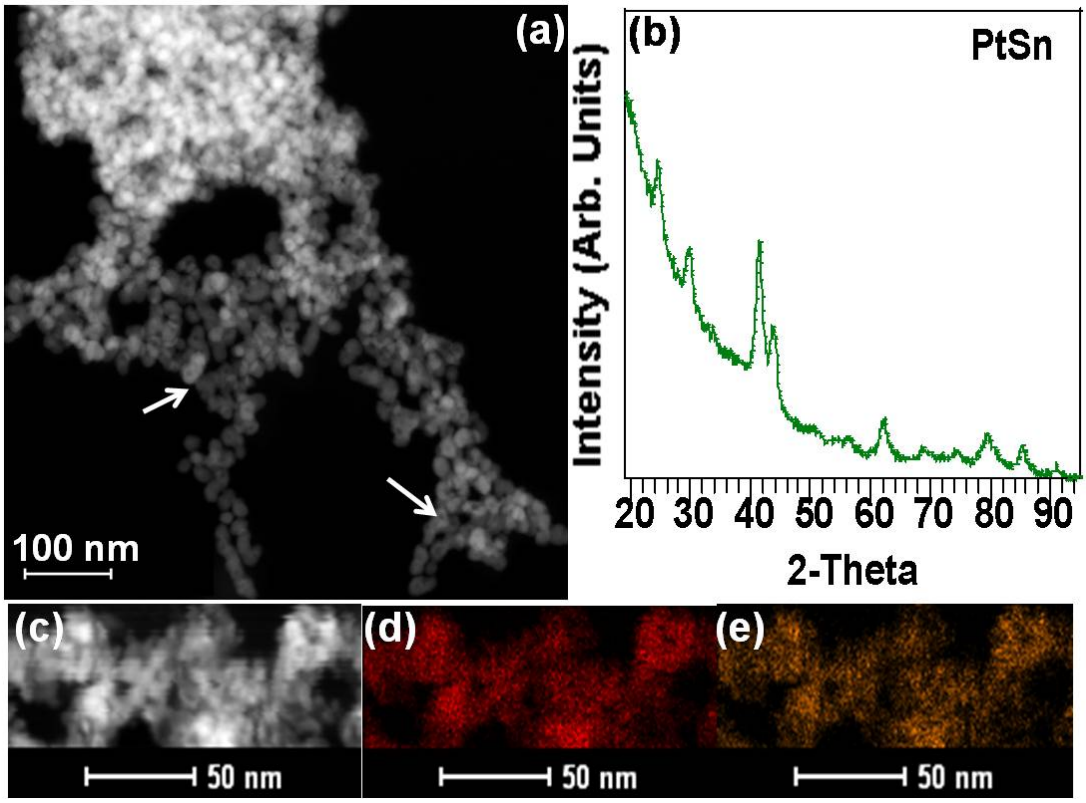

Figure 20. (a) STEM-HAADF image of PtSn particles synthesized by "conversion chemistry". Arrows indicate hollow particles, (b) typical powder X-ray diffraction pattern of PtSn with the NiAs structure, (c) PtSn nanoparticles synthesized using 400 mg of PVP (MW = 40, 000), (d) STEM elemental mapping of Sn L series and (e) STEM elemental mapping of Pt L series.

a SnO_2 shell around the particles. TEM images in Figure 21a show highly crystalline PtSn nanoparticles with the inset showing a high magnification image of a hollow PtSn nanoparticle. The d spacing was found to be 3.01 Å which corresponds well to the bulk value (d_{-101} = 2.98 Å). Figure 20b shows an EDS spectrum of the cluster of PtSn nanoparticles in Figure 21a with stoichiometry of 58.56: 42.44 atomic % percent Sn:Pt. The stoichiometry of the cluster is close to 1:1 when considering that the instrumental error of the EDS detector is 5% and the possibility that there may be a small tin oxide shell.

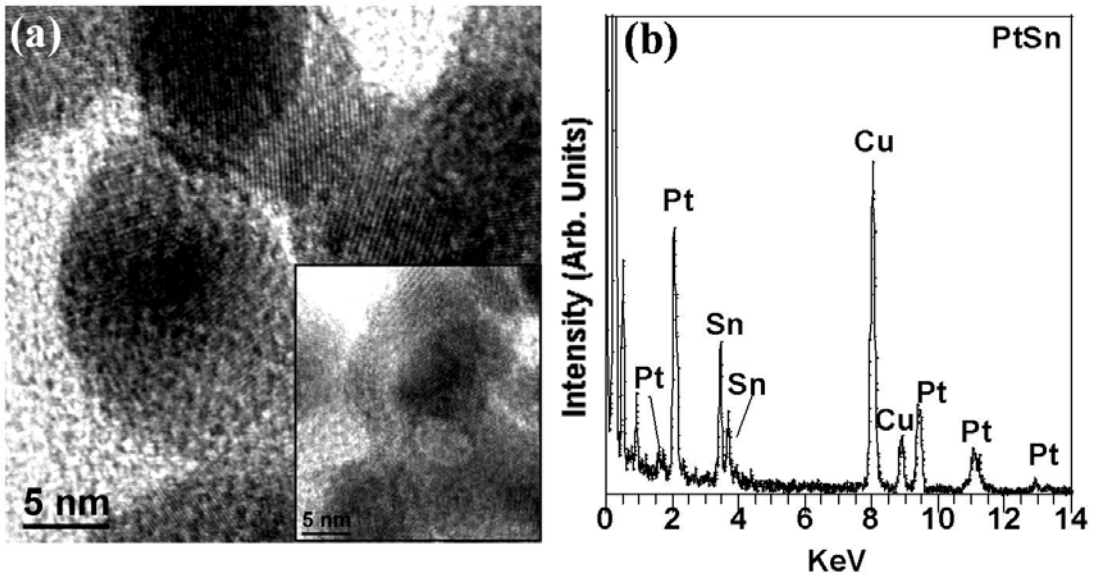

Figure 21. (a) High resolution TEM images of PtSn with d = 3.01 Å; inset: hollow particle of PtSn, (b) EDS spectrum of PtSn nanoparticles in (a).

When forty different areas of clusters of PtSn nanoparticles were analysed by EDS, the average ratio of Sn: Pt was found to be 57.54 ± 1.56: 42.49 ± 1.58 atomic %. The minimum Sn atomic % was 54.41 and the maximum was 60.85 atomic %. The minimum

Pt atomic % was 39.15 and the maximum was 45.59 atomic %. These data show collectively that PtSn particles synthesized by the polyol method are homogeneous, but the deviation from 1:1 stoichiometry cannot be explained in terms of the bulk phase diagram since an oxide shell was observed in other studies using the polyol synthetic procedure. However, a more detailed study must be undertaken to understand the phase diagram of these nanoparticles by synthesizing discrete PtSn particles with no polymer. This could be done by reacting Sn with Pt nanoparticles supported on SiO_2 or carbon. In a SiO_2 matrix, the particles will not form elongated networks and will facilitate the size correlation with the composition.

Transmission Electron Microscopy of $AuCu_3$

$AuCu_3$ nanoparticles synthesized by the polyol process were also found to be unstable under the TEM beam. The nanoparticles were covered by a layer of polymer. When the nanoparticles were drop cast on a holey carbon Ni grid and plasma cleaned for 15 seconds, the samples were stable for single particle STEM EDS analysis. Figure 22a shows representative XRD pattern for $L1_2$ type $AuCu_3$ nanoparticles synthesized by the polyol method. $AuCu_3$ nanoparticles ranged in size from 5-20 nm (Figure 22b) with some networks of particles also observed (Figure 22c). The particles are highly crystalline with no observable impurities by XRD. Figure 22c shows a typical STEM-HAADF image taken for the $AuCu_3$ nanoparticles on a holey carbon Ni grid. The arrows indicate particles where single particle STEM-EDS measurements were taken. Brighter areas indicate differences in the height of the specimen. Figure 22d shows a

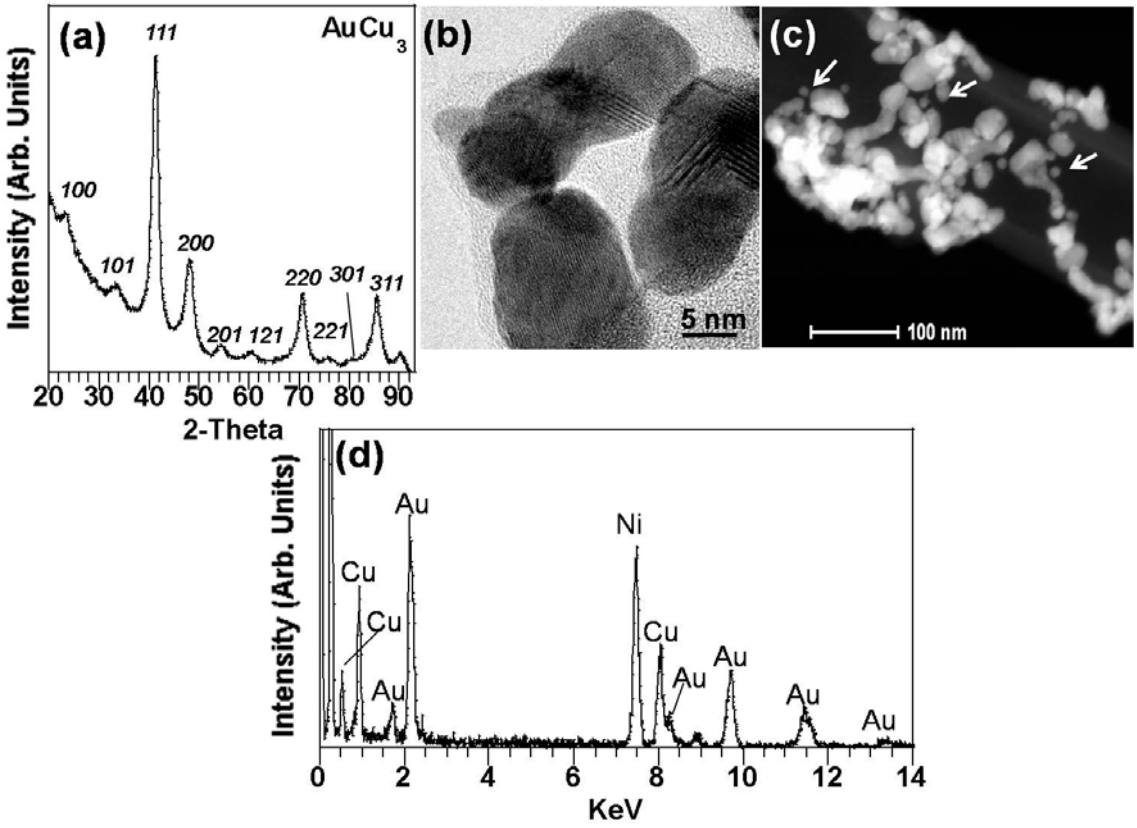

Figure 22. (a) XRD pattern of $AuCu_3$ nanoparticles with $L1_2$ type structure. (b) TEM image of $AuCu_3$ nanoparticles, (c) STEM-HAADF image of $AuCu_3$ on Ni Holey carbon grid, (d) EDS spectrum of large area of $AuCu_3$ nanoparticles with a stoichiometry of 41.12: 58.88 Cu:Au.

typical EDS spectrum taken from a larger area of particles with a ratio of 41.12 : 58.88 Cu: Au atomic %.

Figure 23a shows another STEM HAADF image of $AuCu_3$ nanoparticles indicating that the specimen was homogenous throughout. The bright areas in the STEM-HAADF images are due to specimen height. There was minimal drift observed in $AuCu_3$ specimen as shown by the drift corrected image (Figure 23b). The reduction of drift as compared to the PtSn sample may be attributed to the use of less polymer (100

mg PVP, MW = 630, 000), the high temperatures needed to form the $AuCu_3$ intermetallic (310°C compared to 250°C for PtSn) temperatures where the polymer can decompose, and the removal of some of the polymer due to the plasma cleaner. Au and Cu elemental maps in Figure 23c and Figure 23d show uniform distribution of Au and Cu throughout the specimen. The average composition found for 17 particles was 59.55 ± 4.70: 40.45 ± 6.31 Cu: Au atomic % percent using EDS on the JEOL 2010F TEM. Maximum atomic % percent found for Cu was 69.27 and the minimum was 51.47 atomic % percent. Maximum atomic % percent found for Au was 57.35 and the minimum was 30.73 atomic % percent. Using the FEI Tecnai TEM with STEM EDS, the average stoichiometry was found to be 31.07 ± 10.34: 68.91 ± 10.38 Cu: Au. Based on these results, it can be concluded that there is a larger error in the composition when using STEM-EDS on the FEI Tecani. Although the STEM-EDS should be a more sensitive analytical technique, in this case, the error was very high and may be due to the small beam size, specimen height, and/or geometry of the specimen that contribute to the low counts.

Cu ranged from 51.47- 69.27 atomic % percent in the 17 particles, however, the data suggest that there is significantly more Au in the specimen. No Au impurities were observed by XRD and there was no evidence of Au nanoparticles by elemental mapping experiments. The possibility that the $AuCu_3$ nanoparticles could have a core-shell structure with an Au shell and $AuCu_3$ core due to surface segregation cannot be eliminated since there is no distinguishing between Au in an $AuCu_3$ core or in an Au shell by elemental mapping experiments. This surface segregation has been predicted

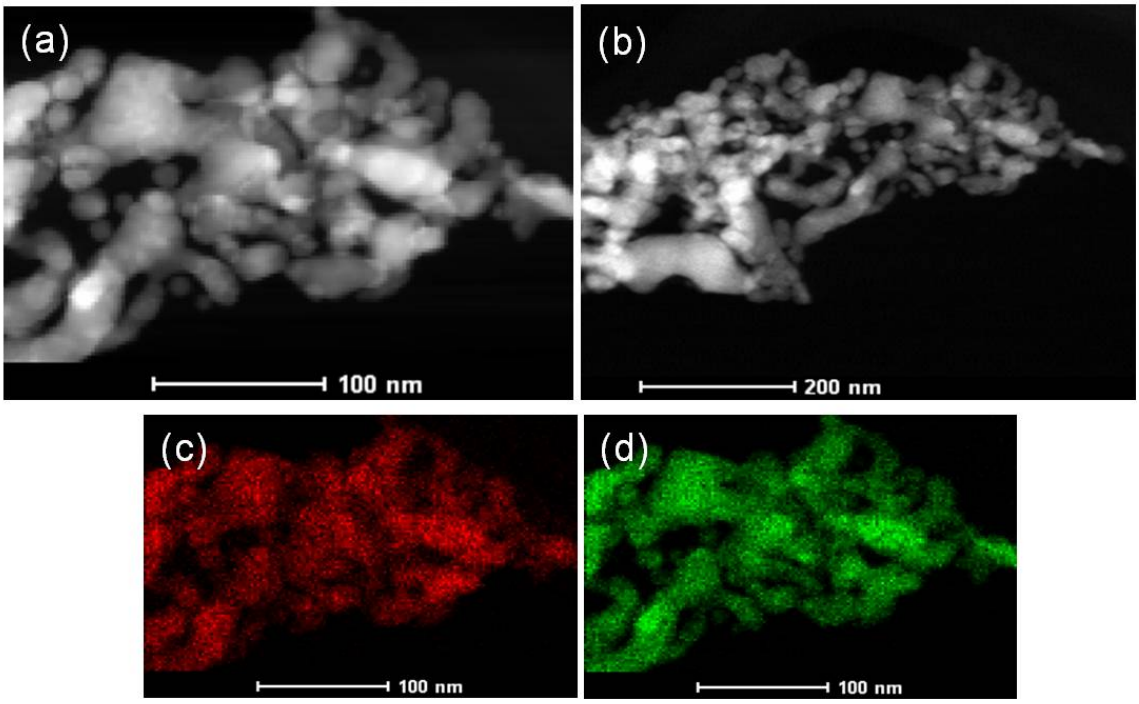

Figure 23.(a) STEM-HAADF image of $AuCu_3$ nanoparticles on Ni holey carbon grid, and (b) drift corrected image of $AuCu_3$ nannoparticles. Elemental maps of $AuCu_3$ nanoparticles (c) Cu K series, and (d) Au M series.

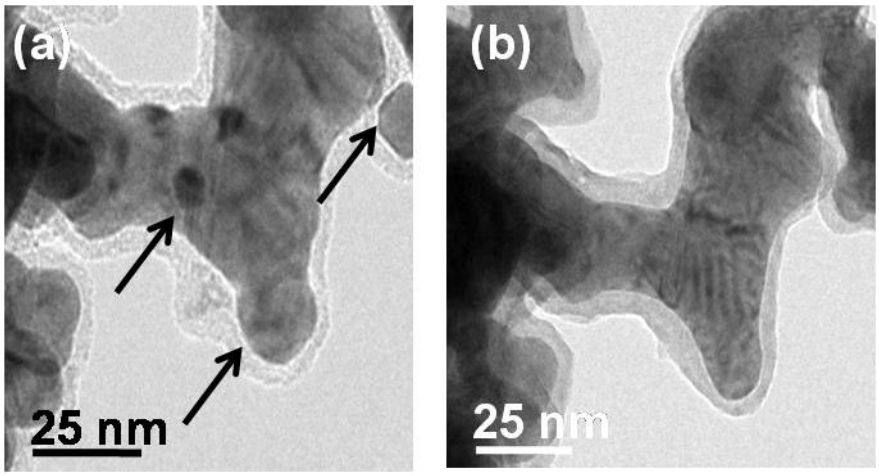

Figure 24. (a) TEM image of $AuCu_3$ nanoparticles before EDS data were collected, (b) TEM image of $AuCu_3$ nanoparticles after EDS data were collected. Arrows indicate areas where some melting is observed.

with theoretical models also suggesting that the Au segregates to the surface in $AuCu_3$ and other AuCu alloys.[145] Depending on the thickness of the Au shell/core, the diffraction intensity may be too weak or broad to be observed in a XRD pattern. While these experiments are instructive and give some insight to the possible structure and composition, no conclusion can be reached as to whether the variance in the composition is attributed to accommodation of a larger atomic % percent of Au in the $L1_2$ structure.

Figures 24a and 24b images show $AuCu_3$ nanoparticles before and after EDS data were collected on the specimen. Melting was observed in the $AuCu_3$ specimen due to heating by the electron beam and changes in the morphology of the nanoparticles are clearly visible (as indicated by the arrows). This intense heat may result in a phase transition from the $L1_2$ to the fcc structure which might explain some phase segregation. Since ED experiments were not conducted in tandem with the EDS experiments and since this transition occurs above 400 °C in thin films, the idea is speculative. Future experiments should include surface studies such as X-ray photoelectron spectroscopy and Auger electron spectroscopy to determine whether a phase transition is occurring and whether a core-shell structure could account for the excess Au present.

CONCLUSION

Because the particles were coated heavily with polymer, they were unstable under the TEM at high magnifications and variations on this synthetic procedure were used to minimize beam instability. Another problem that was encountered in the PtSn system was that the particles resulting from this procedure were highly irregular and networked. The high amounts of polymer made single particle EDS experiments

inconclusive because image shifting due to beam instability made it impossible to determine what particle was being analyzed. Problems with beam stability can be eliminated by synthesizing the nanoparticles without polymer on a support such as SiO_2 or carbon.

EDS data from areas of many nanoparticles at lower magnifications indicate that PtSn nanoparticles are homogenous, however, the deviation from 1:3 Au: Cu stoichiometry could not be attributed to deviation from the bulk phase diagram, although the XRD shows that the structure is the $L1_2$. This suggests that the Au/Cu system deviates significantly from the stoichiometry for the $L1_2$ bulk phase diagram. However, several questions have yet to be answered as to whether a phase transition occurs under the intense heat of the electron beam in these particles. No phase segregation was observed by elemental mapping but more studies on correlating the size and composition will give more insight into the phase diagrams of nanoscale solids. These studies should also be coupled with surface techniques such as X-ray photoelectron spectroscopy and Auger electron spectroscopy to understand if phase segregation is occurring.

CHAPTER V

SUMMARY AND CONCLUSIONS

Low temperature solution methods provide a straightforward framework for expanding the compositional and morphological complexity that is achievable in nanocrystalline solids versus bulk solid state chemistry. While the focus is on generating nanocrystals, these synthetic concepts are also interesting from a solid-state chemistry perspective where the generation of nanoscale solids is not the goal. The ability to carry out reactions on solids using low-temperature solution chemistry techniques, in a regime where solid–solid diffusion is not the rate limiting step in the formation of a product phase, has the potential to generate non-equilibrium solids that cannot be formed, or are not stable, using more traditional high-temperature methods.

In chapter II, a room temperature solution method was developed to synthesize hollow alloyed nanoparticles of CoPt and NiPt. The procedure used Co and Ni nanoparticles that were generated in-situ as morphological templates to produce hollow nanoparticles. This strategy is analogous to work by Xia and co-workers,[55] where the mechanism for the formation of hollow spheres using nanoparticle templates is thought to occur through galvanic replacement reactions. While intermetallic hollow nanoparticles could not be accessed at room temperature in water, a two step process was developed in which Pb/Pt hollow nanoparticles were synthesized in water and subsequently heated to 120°C in TEG resulted in hollow intermetallic PbPt with the NiAs- structure type. These reactions serve as nanoscale conversion chemistry pathways

to generate both alloy and intermetallic hollow particles for applications such as high surface area catalysts.

Chapter III highlights a low temperature solution route that uses n-butyllithium as a reducing agent to access metastable intermetallic nanoparticles of Au_3M, where M = Fe, Co, Ni. The nanoparticles were characterized by EDS, XRD, and single particle electron diffraction. NBED and SAED show superlattice reflections which provide evidence that the particles adopt the *$L1_2$* structure type which has not been previously observed in isolatable samples in these systems. Through aliquots taken from the Au_3Co system at various temperatures, insight into the reaction was gained, which shows evidence that these reactions occur via a nanoscale conversion pathway. This is analogous to $AuCuSn_2$ intermetallic nanocrystals synthesized in solution which also follow a similar reaction pathway, where the single metal nanoparticle nucleates first and is converted into the final ternary intermetallic compound via diffusion.[77] This work is important because it provides a technique to synthesize metastable solids that have been elusive using traditional solid state chemistry.

In chapter IV, PtSn and $AuCu_3$ nanoparticles, synthesized by the modified polyol process, were studied by EDS in order to determine whether there was variation in composition from particle to particle. STEM data for for PtSn suggests that the samples are homogeneous however the composition found by EDS experiments was found to deviate from the 1:1 stoichiometry found in bulk for a NiAs structure type. This could be attributed to SnO_2 shell, but the data were inconclusive in imaging a SnO_2 shell due to beam instability from the PVP stabilizer. From EDS experiments, the stoichiometry

found for $L1_2$ type $AuCu_3$ structure deviates from the 1:3 Au:Cu ratio. The higher atomic % of Au in $L1_2$ type $AuCu_3$ could be a result of $AuCu_3$ core @ Au shell structure. $AuCu_3$ is known to undergo an $L1_2$ to fcc phase transition where the overall structure is ordered but can accommodate disorder at the antiphase boundaries. Because of melting observed this could be occurring in the samples. Since in-situ ED patterns were not taken during these experiments, further work to determine whether there is disorder in the nanoparticles or surface segregation would be necessary. This study only begins to look at the complexity of nanoscale phase diagrams and more experiments must be undertaken to provide a comprehensive description of the variables that lead to the equilibrium states or phase diagrams in nanoscale solids.

Taken together, these solution chemistry techniques are expanding the synthetic toolbox available to solid-state chemists, providing low-temperature strategies for the synthesis of a range of classes of solids and successfully yielding new and metastable solids in a few systems to date. These synthetic procedures are likely to lead to the discovery of new solids and the stabilization of traditionally high-temperature or high-pressure phases under near-ambient conditions. Expansion of these ideas to other classes of solids will be important for accessing a more diverse library of complex nanocrystal systems for advanced scientific studies and emerging applications as well as providing access to nanocrystals and solids with previously unattainable morphologies, compositions, and crystal structures.

REFERENCES

(1) Alivisatos, A. P. *J. Phys. Chem.* **1996**, *100*, 13226-13239.

(2) Jain, P.; Huang, X.; El-Sayed, I.; El-Sayed, M. *Plasmonics* **2007**, *2*, 107-118.

(3) Hu, M.; Chen, J.; Li, Z.-Y.; Au, L.; Hartland, G. V.; Li, X.; Marquez, M.; Xia, Y. *Chem. Soc. Rev.* **2006**, *35*, 1084-1094.

(4) Daniel, M. C.; Astruc, D. *Chem. Rev.* **2004**, *104*, 293-346.

(5) Liu, X.; Bauer, M.; Bertagnolli, H.; Roduner, E.; van Slageren, J.; Phillipp, F. *Phys. Rev. Lett.* **2006**, *97*, 253401-4.

(6) Michael, F.; Gonzalez, C.; Mujica, V.; Marquez, M.; Ratner, M. A. *Phys. Rev. B* **2007**, *76*, 224409-6.

(7) Burda, C.; Chen, X.; Narayanan, R.; El-Sayed, M. A. *Chem. Rev.* **2005**, *105*, 1025-1102.

(8) Astruc, D.; Lu, F.; Aranzaes, J. R. *Angew. Chem. Int. Ed.* **2005**, *44*, 7852-7872.

(9) Wu, B.; Heildelberg, A.; Boland, J. J. *Nat. Mater.* **2005**, *4*, 525-529.

(10) Li, X.; Gao, H.; Murphy, C. J.; Caswell, K. K. *Nano Lett.* **2003**, *3*, 1495-1498.

(11) Darling, S. B.; Bader, S. D. *J. Mater. Chem.* **2005**, *15*, 4189-4195.

(12) Li, F.; Son, D.-I.; Ham, J.-H.; Kim, B.-J.; Jung, J. H.; Kim, T. W. *Appl. Phys. Lett.* **2007**, *91*, 162109-3.

(13) Lee, H.; Yu, M. K.; Park, S.; Moon, S.; Min, J. J.; Jeong, Y. Y.; Kang, H. W.; Jon, S. *J. Am. Chem. Soc.* **2007**, *129*, 12739-12745.

(14) Mornet, S.; Vasseur, S.; Grasset, F.; Duguet, E. *J. Mater. Chem.* **2004**, *14*, 2161-2175.

(15) Lacava, L. M.; Garcia, V. A. P.; Kuckelhaus, S.; Azevedo, R. B.; Lacava, Z. G. M.; Silva, O.; Pelegrini, F.; Gansau, C.; Buske, N.; Morais, P. C. *J. Appl. Phys.* **2003**, *93*, 7563-7565.

(16) Raimondi, F.; Scherer, G. G.; Kötz, R.; Wokaun, A. *Angew. Chem. Int. Ed.* **2005**, *44*, 2190-2209.

(17) Yao, X.; Wu, C.; Du, A.; Zou, J.; Zhu, Z.; Wang, P.; Cheng, H.; Smith, S.; Lu, G. *J. Am. Chem. Soc.* **2007**, *129*, 15650-15654.

(18) Kamat, P. V. *J. Phys. Chem. C* **2007**, *111*, 2834-2860.

(19) Reetz, M. T.; Breinbauer, R.; Wanninger, K. *Tet. Lett.* **1996**, *37*, 4499.

(20) Li, Y.; El-sayed, M. A. *J. Phys. Chem. B* **2001**, *105*, 8938.

(21) Teng, X.; Yang, H. *J. Am. Chem. Soc.* **2003**, *125*, 14559-14563.

(22) Li, Y.-J.; Huang, W.-J.; Sun, S.-G. *Angew. Chem. Int. Ed.* **2006**, *45*, 2537-2539.

(23) Chumanov, G.; Sokolov, K.; Gregory, B. W.; Cotton, T. M. *J. Phys. Chem.* **1995**, *99*, 9466-9471.

(24) Urban, J. J.; Talapin, D. V.; Shevchenko, E. V.; Kagan, C. R.; Murray, C. B. *Nat. Mater.* **2007**, *6*, 115-121.

(25) Cademartiri, L.; Freymann, G.; Arsenault, A. C.; Bertolotti, J.; Wiersma, D. S.; Kitaev, V.; Ozin, G. A. *Small* **2005**, 1184.

(26) Xu, X.; Stevens, M.; Cortie, M. B. *Chem. Mater.* **2004**, *16*, 2259.

(27) Crisp, M. T.; Kotov, N. A. *Nano Lett.* **2003**, *3*, 173-177.

(28) Jiang, P.; Bertone, J. F.; Colvin, V. L. *Science* **2001**, *291*, 453-457.

(29) Stein, A.; Schroden, R. C. *Curr. Opin. Solid State Mater. Sci.* **2001**, *5*, 553-564.

(30) Schaak, R. E.; Sra, A. K.; Leonard, B. M.; Cable, R. E.; Bauer, J. C.; Han, Y. F.; Means, J.; Teizer, W.; Vasquez, Y.; Funck, E. S. *J. Am. Chem. Soc.* **2005**, *127*, 3506-3515.

(31) Munoz, J. E.; Cercantes, J.; Esparza, R.; Rosas, G. *J. Nanopart Res.* **2007**, *9*, 945-950.

(32) Koch, C. C.; Whittenberger, J. D. *Intermetallics* **1996**, *4*, 339-355.

(33) Milani, P.; deHeer, W. A. *Rev. Sci. Instrum.* **1990**, *61*, 1835-1838.

(34) Raffi, M.; Rumaiz, A.; Hasan, M. M.; Shah, S. I. *J. Mater. Res.* **2007**, *22*, 3378-3384.

(35) Haubold, T.; Bohn, R.; Birringer, R.; Gleiter, H. *Mater. Sci. Eng.* **1992**, *A153*, 679-683.

(36) Pivin, J. C.; Garcia, M. A.; Llopis, J.; Hofmeister, H. *Nucl. Instr. and Meth. in Phys. Res. B* **2002**, *191*, 794-799.

(37) Mishra, Y. K.; Mohaptra, S.; Kabirag, D.; Mohanta, B.; Lalla, N. P.; Pivin, J. C.; Avasthi, D. K. *Script., Mater.* **2007**, *56*, 629-632.

(38) Gurav, A.; Kodas, T.; Pluym, T.; Xiong, Y. *Aerosol Sci. Technol.* **1993**, *19*, 411-452.

(39) Pratsinis, S. E. *Prog. in Energy Combust. Sci.* **1998**, *24*, 197-219.

(40) Nie, J. C.; Yamasaki, H.; Mawatari, Y. *Phys. Rev. B* **2004**, *70*, 195421/1-195421/11.

(41) Cushing, B. L.; Kolesnichenko, V. L.; O'Connor, C. J. *Chem. Rev.* **2004**, *104*, 3893-3946.

(42) Roucoux, A.; Schulz, J.; Patin, H. *Chem. Rev.* **2002**, *102*, 3757-3778.

(43) Dumestre, F.; Chaudret, B.; Amiens, C.; Fromen, M.-C.; Casanove, M.-J.; Renaud, P.; Zurcher, P. *Angew. Chem. Int. Ed.* **2002**, *41*, 4286-4289.

(44) Sun, S.; Murray, C. B.; Weller, D.; Folks, L.; Moser, A. *Science* **2000**, *287*, 1989.

(45) Gul, I. H.; Ahmed, W.; Maqsood, A. *J. Magn. Magn. Mater* **2008**, *320*, 270.

(46) Pileni, M. P. *Langmuir* **1997**, *13*, 3266-3276.

(47) Pileni, M. P. *Nat. Mater.* **2003**, *2*, 145.

(48) Rajamathi, M.; Seshadri, R. *Curr. Opin. Solid State Mater. Sci.* **2002**, *6*, 337-345.

(49) Chaudret, B. *Top. Organomet. Chem.* **2005**, *16*, 233-259.

(50) Hanrath, T.; Korgel, B. A. *J. Am. Chem. Soc.* **2004**, *126*, 15466-15472.

(51) Stowell, C. A.; Korgel, B. A. *Nano Lett.* **2005**, *5*, 1203-1207.

(52) Zhang, T.; Ge, J.; Hu, Y.; Yin, Y. *Nano Lett.* **2007**, *7*, 3203-3207.

(53) Puntes, V. F.; Krishnan, K. M.; Alivisatos, A. P. *Science* **2001**, *291*, 2115-2117.

(54) Scher, E. C.; Manna, L.; Alivisatos, A. P. *Phil. Trans. R. Soc. Lond. A* **2003**, *361*, 241-257.

(55) Sun, Y.; Xia, Y. *Science* **2002**, *298*, 2176-2179.

(56) Sun, Y.; Mayers, B. T.; Xia, Y. *Nano Lett.* **2002**, *2*, 481-485.

(57) Chen, J.; Herricks, T.; Xia, Y. *Angew. Chem. Int. Ed.* **2005**, *44*, 2589-2592.

(58) Nikhil , R. J. *Small* **2005**, *1*, 875-882.

(59) Park, J.; An, K.; Hwang, Y.; Park, J.-G.; Noh, H.-J.; Kim, J.-Y.; Park, J.-H.; Hwang, N.-M.; Hyeon, T. *Nat. Mater.* **2004**, *3*, 891-895.

(60) Zheng, N.; Fan, J.; Stucky, G. D. *J. Am. Chem. Soc.* **2006**, *128*, 6550-6551.

(61) Brust, M.; Walker, A.; Bethell, D.; Schiffrin, D. J.; Whyman, R. *J. Chem. Soc. Chem. Commun.* **1994**, 801.

(62) Seo, D.; Park, J. C.; Song, H. *J. Am. Chem. Soc.* **2006**, *128*, 14863-14870.

(63) Chang, G.; Oyama, M.; Hirao, K. *Acta Mater.* **2007**, *55*, 3453-3456.

(64) Xiong, Y.; McLellan, J. M.; Chen, J.; Yin, Y.; Li, Z. Y.; Xia, Y. *J. Am. Chem. Soc.* **2005**, *127*, 17118-17127.

(65) Washio, I.; Xiong, Y.; Yin, Y.; Xia, Y. *Adv. Mater.* **2006**, *18*, 1745-1749.

(66) Puntes, V. F.; Zanchet, D.; Erdonmez, C. K.; Alivisatos, A. P. *J. Am. Chem. Soc.* **2002**, *124*, 12874.

(67) Wiley, B.; Sun, Y.; Xia, Y. *Acc. Chem. Res.* **2007**, *40*, 1067-1076.

(68) Kim, F.; Connor, S.; Song, H.; Kuykendall, T.; Yang, P. *Angew. Chem. Int. Ed.* **2004**, *43*, 3673-3677.

(69) Lim, B.; Xiong, Y.; Xia, Y. *Angew. Chem. Int. Ed.* **2007**, *46*, 9279.

(70) Herricks, T.; Chen, J.; Xia, Y. *Nano Lett.* **2004**, *4*, 2367-2371.

(71) Sau, T. K.; Murphy, C. J. *J. Am. Chem. Soc.* **2004**, *126*, 8648-8649.

(72) Chen, S.; Wang, Z. L.; Ballato, J.; Foulger, S. H.; Carroll, D. L. *J. Am. Chem. Soc.* **2003**, *125*, 16186-16187.

(73) Murphy, C. J.; Sau, T. K.; Gole, A. M.; Orendorff, C. J.; Gao, J.; Gou, L.; Hunyadi, S. E.; Li, T. *J. Phys. Chem. B* **2005**, *109*, 13857-13870.

(74) Murphy, C. J.; Gole, A. M.; Hunyadi, S. E.; Orendorff, C. J. *Inorg. Chem.* **2006**, *45*, 7544-7554.

(75) Sun, Y.; Tao, Z.; Chen, J.; Herricks, T.; Xia, Y. *J. Am. Chem. Soc.* **2004**, *126*, 5940-5941.

(76) Leonard, B. M.; Bhuvanesh, N. S. P.; Schaak, R. E. *J. Am. Chem. Soc.* **2005**, *127*, 7326-7327.

(77) B. M. Leonard; R. E. Schaak *J. Am. Chem. Soc.* **2006**, *128*, 11475.

(78) Roychowdhury, C.; Matsumoto, F.; Mutolo, P. F.; Abruna, H. D.; DiSalvo, F. J. *Chem. Mater.* **2005**, *17*, 5871-5876.

(79) Maksimuk, S.; Yang, S.; Peng, Z.; Yang, H. *J. Am. Chem. Soc.* **2007**, *129*, 8684-8685.

(80) Chou, N. H.; Schaak, R. E. *J. Am. Chem. Soc.* **2007**, *129*, 7339.

(81) Chou, N. H.; Schaak, R. E. *Chem. Mater.* **2008**, *20*, 2081-2085.

(82) Lang, A.; Jeitschko, W. Z. *Metallkunde* **1996**, *87*, 759-764.

(83) Kanatzidis, M. G.; Pottgen, R.; Jeitschko, W. *Angew. Chem., Int. Ed. Engl.* **2005**, *44*, 6996-7023.

(84) Mathiowitz, E.; Jacob, J. S.; Jong, Y. S.; Carino, G. P.; Chickering, D. E.; Chaturvedi, P.; Santos, C. A.; Vijayaraghavan, K.; Montgomery, S.; Bassett, M.; Morrell, C. *Nature* **1997**, *386*, 410-414.

(85) David, E. B. *Angew. Chem. Int. Ed.* **1999**, *38*, 2870- 2872.

(86) Marinakos, S. M.; Novak, J. P.; Brousseau, L. C.; House, A. B.; Edeki, E. M.; Feldhaus, J. C.; Feldheim, D. L. *J. Am. Chem. Soc.* **1999**, *121*, 8518-8522.

(87) Marinakos, S. M.; Anderson, M. F.; Ryan, J. A.; Martin, L. D.; Feldheim, D. L. *J. Phys. Chem. B* **2001**, *105*, 8872-8876.

(88) Tartaj, P.; Morales, M. d. P.; Veintemillas-Verdaguer, S.; Gonzalez-Carreno, T.; Serna, C. J. *J. Phys. D: Appl. Phys.* **2003**, R182.

(89) Kim, S. W.; Kim, M.; Lee, W. Y.; Hyeon, T. *J. Am. Chem. Soc.* **2002**, *124*, 7642-7643.

(90) Oldenburg, S. J.; Averitt, R. D.; Westcott, S. L.; Halas, N. J. *Chem. Phys. Lett.* **1998**, *288*, 243-247.

(91) Cochran, J. K. *Curr. Opin. Solid State Mater. Sci.* **1998**, *3*, 474-479.

(92) Sershen, S. R.; Westcott, S. L.; Halas, N. J.; West, J. L. *J. Biomed. Mater. Res.* **2000**, *51*, 293-298.

(93) Antonietti, M., editor, Caruso, F. In *Colloid Chemistry II*; Springer-Verlag: Berlin 2003 , p 145-168.

(94) Liu, J. B.; Dong, W.; Zhan, P.; Wang, S. Z.; Zhang, J. H.; Wang, Z. L. *Langmuir* **2005**, *21*, 1683-1686.

(95) Sun, Y.; Mayers, B.; Xia, Y. *Adv. Mater.* **2003**, *15*, 641-646.

(96) Selvakannan, P. R.; Sastry, M. *Chem. Commun.* **2005**, 1684-1686.

(97) Metraux, G. S.; Cao, Y. C.; Jin, R.; Mirkin, C. A. *Nano Lett.* **2003**, *3*, 519-522.

(98) Sun, Y.; Wiley, B.; Li, Z. Y.; Xia, Y. *J. Am. Chem. Soc.* **2004**, *126*, 9399-9406.

(99) Liang, H.-P.; Guo, Y.-G.; Zhang, H.-M.; Hu, J.-S.; Wan, L.-J.; Bai, C.-L. *Chem. Commun.* **2004**, 1496-1497.

(100) Scott, R. W. J.; Wilson, O. M.; Oh, S. K.; Kenik, E. A.; Crooks, R. M. *J. Am. Chem. Soc.* **2004**, *126*, 15583-15591.

(101) Lang, H.; Maldonado, S.; Stevenson, K. J.; Chandler, B. D. *J. Am. Chem. Soc.* **2004**, *126*, 12949-12956.

(102) Mulvaney, P. *Langmuir* **1996**, *12*, 788-800.

(103) Yin, Y.; Erdonmez, C.; Aloni, S.; Alivisatos, A. P. *J. Am. Chem. Soc.* **2006**, *128*, 12671-12673.

(104) Lu, X.; Tuan, H.-Y.; Chen, J.; Li, Z.-Y.; Korgel, B. A.; Xia, Y. *J. Am. Chem. Soc.* **2007**, *129*, 1733-1742.

(105) Sastry, M.; Swami, A.; Mandal, S.; Selvakannan, P. R. *J. Mater. Chem.* **2005**, *15*, 3161-3174.

(106) Liang, H. P.; Wan, L. J.; Bai, C. L.; Jiang, L. *J. Phys. Chem. B* **2005**, *109*, 7795-7800.

(107) Liang, H. P.; Zhang, H.-M.; Hu, J.-S.; Guo, L. J.; Wan, L. J.; Bai, C. L. *Angew. Chem. Int. Ed.* **2004**, *43*, 1540.

(108) Zeng, J.; Huang, J.; Lu, W.; Wang, X.; Wang, B.; Zhang, S.; Hou, J. *Adv. Mater.* **2007**, *19*, 2172-2176.

(109) Chen, J.; Wiley, B.; McLellan, J. M.; Xiong, Y.; Li, Z.-Y.; Xia, Y. *Nano Lett.* **2005**, *5*, 2058-2068.

(110) Chen, J.; McLellan, J. M.; Siekkinen, A.; Xiong, Y.; Li, Z.-Y.; Xia, Y. *J. Am. Chem. Soc.* **2006**, *128*, 14776-14777.

(111) Sun, Y.; Xia, Y. *Adv. Mater.* **2004**, *16*, 264-268.

(112) Sun, Y.; Xia, Y. *Nano Lett.* **2003**, *3*, 1569-1572.

(113) Zhang, Q.; Lee, J. Y.; Yang, J.; Boothroyd, C.; Zhang, J. *Nanotechnology* **2007**, *18*, 245605-245613.

(114) Liang, H.-P.; Guo, Y.-G.; Zhang, H.-M.; Hu, J.-S.; Wan, L.-J.; Bai, C.-L. *Chem. Commun.* **2004**, 1496-1497.

(115) Alden, L. R.; Roychowdhury, C.; Matsumoto, F.; Han, D. K.; Zeldovich, V. B.; Abruna, H. D.; DiSalvo, F. J. *Langmuir* **2006**, *22*, 10465-10471.

(116) Lee, Y.-S.; Lim, K.-Y.; Chung, Y.-D.; Whang, C.-N.; Jeon, Y. *Surf. Interf. Anal.* **1999**, *30*, 475-478.

(117) Pastoriza-Santos, I.; Liz-Marzan, L. M. *Langmuir* **2002**, *18*, 2888-2894.

(118) Wang, Y.; Cai, L.; Xia, Y. *Adv. Mater.* **2005**, *17*, 473-477.

(119) Lahr, D. L.; Ceyer, S. T. *J. Am. Chem. Soc.* **2006**, *128*, 1800-1801.

(120) Auten, B. J.; Hahn, B. P.; Vijayaraghavan, G.; Stevenson, K. J.; Chandler, B. D. *J. Phys. Chem. C* **2008**, *112*, 5365-5372.

(121) Mader, S.; Nowick, A. S. *Appl. Phys. Lett.* **1965**, *7*, 57-59.

(122) Lee, Y. P.; Kudryavtsev, Y. V.; Nemoshkalenko, V. V.; Gontarz, R.; Rhee, J. Y. *Phys. Rev. B* **2003**, *67*, 104424.

(123) Canet, F.; Bellouard, C.; Joly, L.; Mangin, S. *Phys. Rev. B* **2004**, *69*, 094402.

(124) Taniyama, T.; Ogawa, R.; Sato, T.; Ohta, E. *Mater. Sci. Eng. A* **1996**, *217-218*, 319-321.

(125) Taniguchi, T.; Yamanaka, K.; Sumioka, H.; Yamazaki, T.; Tabata, Y.; Kawarazaki, S. *Phys. Rev. Lett.* **2004**, *93*, 246605.

(126) Chiang, I.-C.; Chen, D. H. *Adv. Funct. Mater.* **2007**, *17*, 1311-1316.

(127) Sargolzae, M.; Opahle, I.; Richter, M. *Phys. Stat. Sol. (b)* **2006**, *243*, 286-289.

(128) Kong, Y.; Kong, L. T.; Liu, B. X. *J. Phys.: Cond. Matt.* **2006**, 4345.

(129) Reichert, H.; Schops, A.; Ramsteiner, I. B.; Bugaev, V. N.; Shchyglo, O.; Udyansky, A.; Dosch, H.; Asta, M.; Drautz, R.; Honkimaki, V. *Phys. Rev. Lett.* **2005**, *95*, 235703-4.

(130) Wolverton, C.; Zunger, A. *Comput. Mater. Sci.* **1997**, *8*, 107-121.

(131) Takanashi, K.; Mitani, S.; Sano, M.; Fujimori, H.; Nakajima, H.; Osawa, A. *Appl. Phys. Lett.* **1995**, *67*, 1016-1018.

(132) Sato, K.; Bian, B.; Hirotsu, Y. *Jpn. J. Appl. Phys.* **2002**, *41*, L1-3.

(133) Tzu-Hsuan, K.; Jenn-Ming, S.; In-Gann, C.; Teng-Yuan, D.; Weng-Sing, H. *Nanotechnology* **2007**, *18*, 435708.

(134) Yan, H. F.; Guo, H. B.; Shen, Y. X.; Li, J. H.; Liu, B. X. *Acta Mater.* **2006**, *54*, 5293-5304.

(135) Nabika, H.; Akamatsu, K.; Mizuhata, M.; Kajinami, A.; Deki, S. *J. Mater. Chem.* **2002**, *12*, 2408-2411.

(136) He, J. H.; Carosella, C. A.; Hubler, G. K.; Qadri, S. B.; Sprague, J. A. *Phys. Rev. Lett.* **2006**, *96*, 056105-4.

(137) Williams, D. B.; Carter, C. B. *Tranmission Electron Microscopy: Diffraction II*; Plenum Press: New York, 1996.

(138) Zhou, S.; Jackson, G. S.; Eichhorn, B. *Adv. Funct. Mater.* **2007**, *17*, 3099-3104.

(139) Ouyang, G.; Tan, X.; Wang, C. X.; Wang, G. W. *Nanotechnology* **2006**, *17*, 4257.

(140) Shirinyan, A. S.; Gusak, A. M.; Wautelet, M. *Acta Mater.* **2005**, *53*, 5025-5032.

(141) Shirinyan, A. S.; Gusak, A. M. *Philos. Mag.* **2004**, *84*, 579- 593.

(142) Hills, C. W.; Mack, N. H.; Nuzzo, R. G. *J. Phys. Chem. B* **2003**, *107*, 2626-2636.

(143) Bonneaux, J.; Guymont, M. *Intermetallics* **1999**, *7*, 797-805.

(144) Malis, O.; K. F. Ludwig, J. *Phys. Rev. B* **1999**, *60*, 14675.

(145) Bangwei, Z.; Taglauer, E.; Xiaolin, S.; Wangyu, H.; Huiqiu, D. *Phys. Stat. Sol. A* **2005**, *202*, 2686.

(146) Pal, U.; Sanchez Ramirez, J. F.; Liu, H. B.; Medina, A.; Ascencio, J. A. *Appl. Phys. A: Mater. Sci. & Process.* **2004**, *79*, 79-84.

(147) Ascencio, J. A.; Liu, H. B.; Pal, U.; Medina, A.; Wang, Z. L. *Microsc. Res. Techn.* **2006**, *69*, 522.

(148) Sra, A. K.; Ewers, T. D.; Schaak, R. E. *Chem. Mater.* **2005**, *17*, 758-766.

(149) Cable, R. E.; Schaak, R. E. *Chem. Mater.* **2005**, *17*, 6835.

VITA

Yolanda Vasquez received her Bachelor of Science degree in chemistry from The University of Texas at El Paso in 2003, where she was supported by a Minority Access to Research Careers (MARC) fellowship. She entered the chemistry doctoral program at Texas A&M University in September 2003 and was supported by a Pathways to the Doctorate fellowship. She joined the group of Prof. Raymond E. Schaak in October of the same year and received her Doctor of Philosophy degree in December 2008. Her research interests include the synthesis of alloys and intermetallics for fuel cell applications, shape-controlled synthesis of solid state materials, and the assembly of nanoparticles into hierarchical structures.

Ms. Vasquez may be reached at the Department of Chemistry, Texas A&M University, P. O. Box 30012 College Station, TX 77842-3012. Her email is yvasquez@mail.chem.tamu.edu.